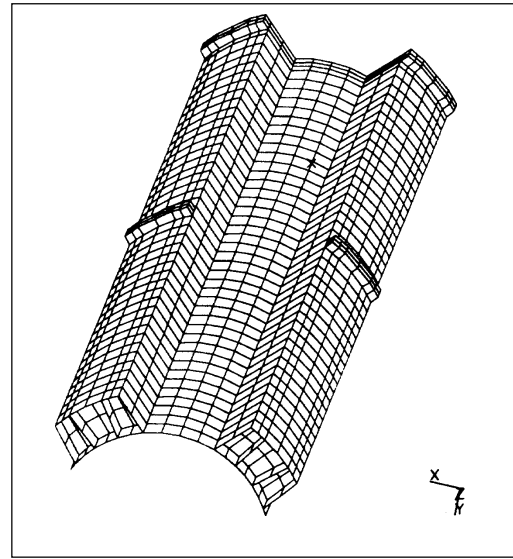


a. Top view.



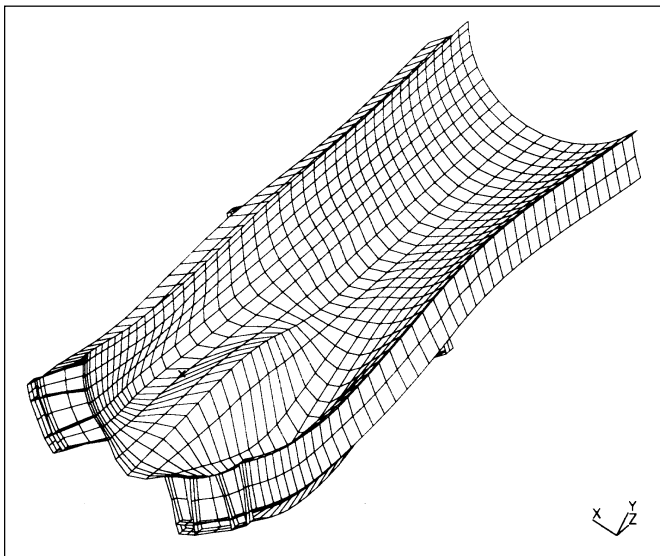
b. Bottom view.

Figure 32. Shell-element finite-element model for Magway.

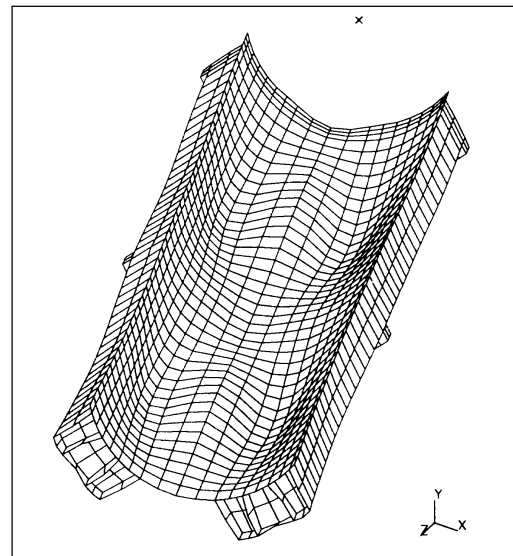
linear-elastic material with an elastic modulus of 68,950 MPa. The LSM winding between the box beams was modeled as the same material and was assumed to be continuously connected to each of the adjacent box beams. It is actually constructed from a composite FRP material and is bolted to the box beams, the details of which could not be found. The assumption of a continuous connection to the box beams may not have been conservative and, therefore, the analytical results should be considered with this in mind.

Since the Magway is two-span continuous, two different static load cases were considered. Load case 1 had only one bogie set in the middle of one span, representing a vehicle at the halfway point across the span. Load case 2 represented a vehicle with its midpoint at the middle Magway support and, thus, had a bogie set near the middle of each span.

Results. The magnified displaced shape from load case 1 is shown in Figure 33a. It had a maximum downward deflection of 2.9 mm in a direc-



a. Load case 1.



b. Load case 2.

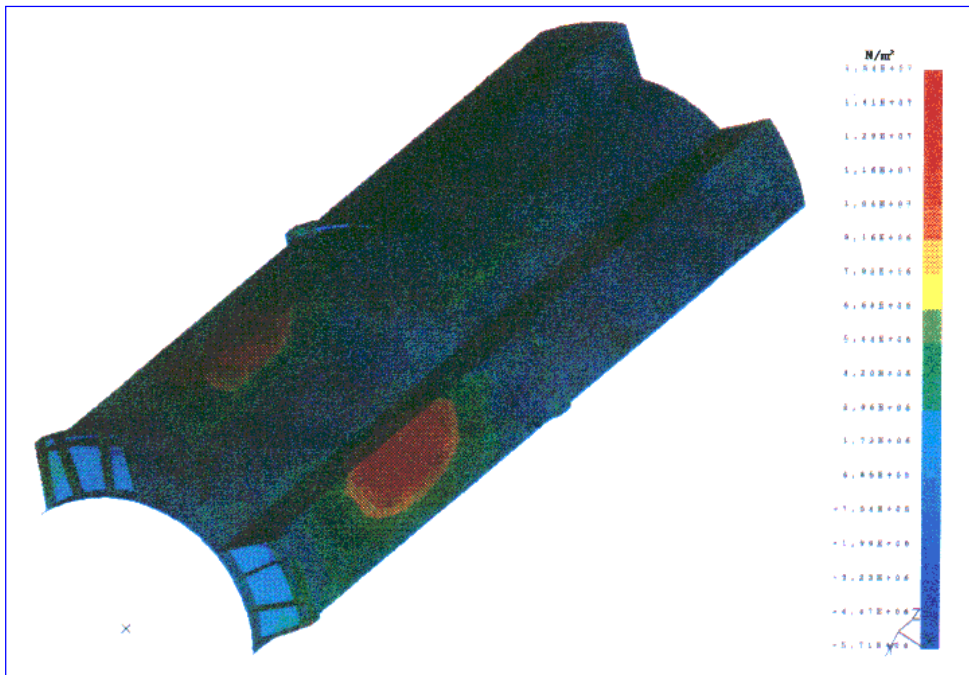
Figure 33. Displaced Magway shape.

tion normal to the vertical axes of the box beams. Figure 33b shows the deflected shaped for load case 2, which produced a maximum displacement of 2.6 mm normal to the box beams. Figure 33a shows that the deflections were somewhat localized and transferred to the bottom plate, mainly

through the longitudinal stiffeners directly beneath the bogies. Although not required on the basis of these analyses, further stiffness could be added to the Magway through additional transverse diaphragms along its length, which would allow more load sharing between the longitudinal



a. Top view.



b. Bottom view.

Figure 34. Maximum principal stresses from Magway dynamic analysis, load case 1.

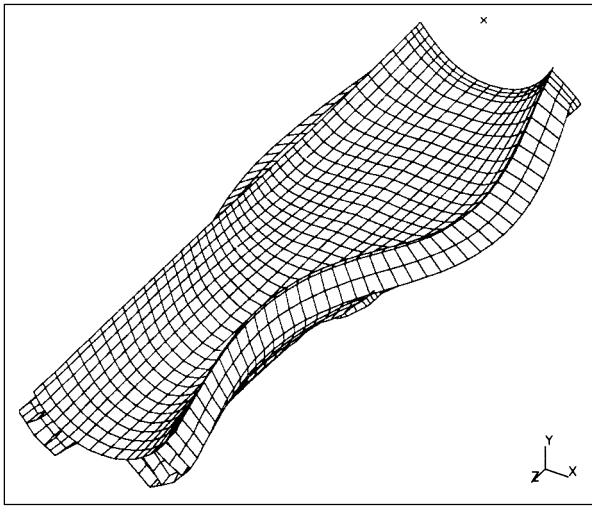
stiffeners. This addition could possibly reduce the required thicknesses for the top and bottom plates (although Magneplane's top-plate thickness is based on magnetic considerations).

Maximum principal stress contours are shown for load case 1 (worst of the two cases) in Figure 34. These stresses were all below 15.4 MPa tension and 5.7 MPa compression. Although no dynamic calculations were performed to determine the cyclic stresses, these low static stresses are well below the 41.40-MPa fatigue limit for Aluminum 6061-T6.

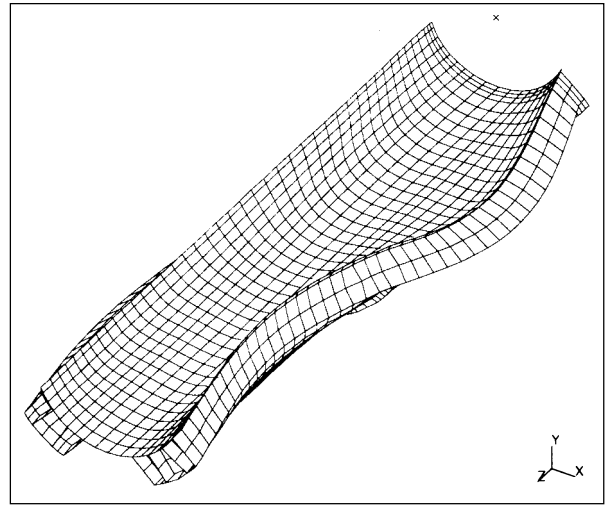
Figure 34 shows that the LSM winding (as modeled) fully shares in the compressive bending stresses at the top of the Magway. Depending upon how it is attached to the box beams, this may

not actually be the case. If it is attached in a way that allows for its unrestrained longitudinal movement, it will not share in any of the longitudinal bending stress of the box beams and the stresses in these beams will be slightly higher than calculated here. However, they will likely still be well within the allowable fatigue limits.

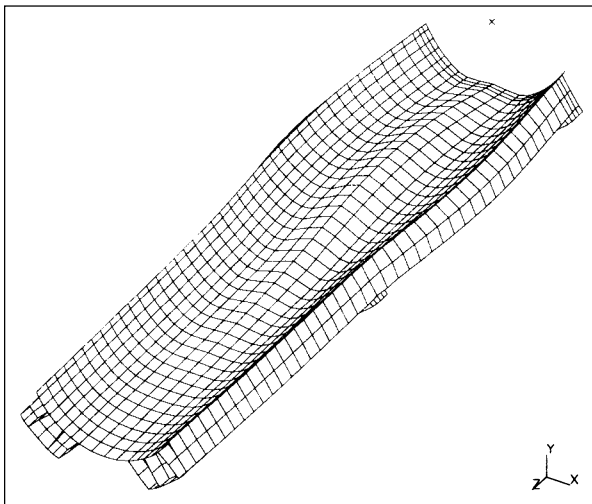
The first four dynamic bending modes are shown in Figure 35. The frequencies of these modes were 30.7, 34.6, 37.7, and 39.3 Hz, respectively. The Magway is much stiffer than the other SCD guideways because of its shorter span and relatively deeper (in relation to span length) section. Because of the Magway's high-frequency response, there will likely be no large dynamic effects from the vehicle passage. This is true even



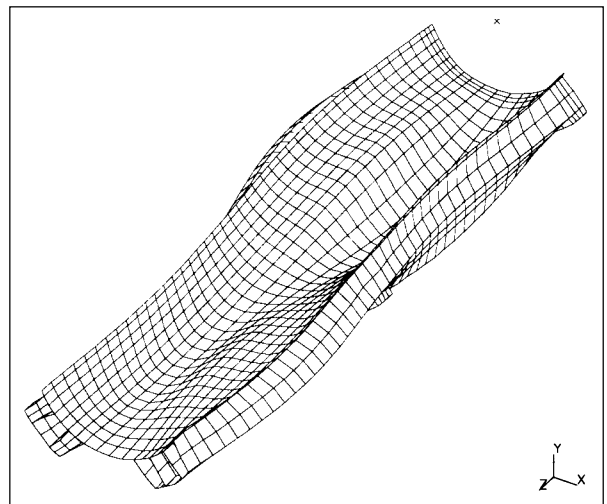
a. First.



b. Second.



c. Third.



d. Fourth.

Figure 35. Dynamic flexural mode for Magway.

though the bogies are spaced far apart, like those on the Foster-Miller vehicle, which had a significant dynamic effect.

Conclusions. The limited analyses tell us that the Magway is a very stiff and well-designed structure. The stresses appear to be low throughout, which is a primary requirement for an aluminum structure under cyclic loading.

Further study of this structure should include a series of dynamic analyses with worst-case vehicular loadings, including guideway curvature. While the stiff Magway will likely prevent much of an increase in the dynamic deflections over the static case, a thorough study of the dynamic stress variations within the structure is necessary to ensure its fatigue durability.

3.2.2 Linear synchronous motor*

Objectives

All of the maglev concepts investigated use guideway-mounted linear synchronous motors (LSMs) to propel the vehicles. These motors present high capital costs, and their power consumption creates the system's highest operating cost. For these reasons, the GMSA team required an LSM model as a performance-evaluation tool. Also, LSM performance data were needed to simulate the operational performance of each concept along specific corridors (see section 3.3.1). The resulting model (LSMPOWER) is able to evaluate both iron-core and air-core LSMs and fulfills both needs.

The specific objectives of this work are:

- To determine the equivalent circuit parameters from the basic size and layout of the guideway-mounted stator winding and vehicle-mounted field windings.
- To determine the required electrical characteristics at the terminals of the LSM to meet the specified thrust conditions.
- To compute the thrust margins required in each concept (i.e., the thrusts required for acceleration and for operation on a grade).
- To compute performance data (power, efficiency, power factor, etc.) at the input to the LSM and at the output of the variable frequency converters located along the guideway.

- To evaluate, from the performance data, the LSM's thrust capability for vehicle acceleration and grade climbing.

Introduction

LSMs consist of two electromagnetic members: the armature and the field. In long-stator systems, the LSM armature, commonly called the stator, is located on the guideway and the field is located on the vehicle. Short-stator systems have these structures reversed.

Electromagnetic suspension (EMS) systems make use of iron structures for both the field and the stator. The saturation of flux density in the iron limits the magnitude of the flux density that can be obtained in the air gap. This limits an EMS to small air gaps, typically of the order of 10 mm. The Grumman SCD's innovative use of superconducting coils in conjunction with the iron-core stator has the potential for increasing the stator-to-field air gap to 40 mm.

Electrodynamic suspension (EDS) systems use air-core structures for both the field and stator. Superconducting field windings on the vehicle are required to achieve the large flux densities required for operating EDS at large air gaps. These air gaps typically operate with a 100- to 200-mm spacing between the stator and the field.

LSMs can be controlled to produce orthogonal forces, for example, forces that act in the longitudinal direction and in the direction perpendicular to the longitudinal. Almost all maglev systems make use of LSMs to achieve either lift and propulsion, or guidance and propulsion. The LSM used in the TR07, for example, provides both lift and propulsive forces. The LSM is similar to its rotary counterpart in that a machine of fixed dimensions and materials produces a finite total force. Trade studies then determine how to apportion the split of the orthogonal forces. Iron-core structures typically produce large vertical forces because of the presence of the iron. On the other hand, the operation of air-core structures can be tailored through their control system to split the force capability from being all longitudinal to all vertical or a combination of both.

The power factor, that is the ratio of power consumed (P) to power applied (S), for LSMs can be significantly less than unity because of the inductance of the motor. The inductance causes LSMs to operate with a lagging power factor. The principal component of inductance in iron-core machines is a result of the magnetic circuit of the iron. For air-core machines, the relatively large size

* Written by Frank L. Raposa, Consulting Engineer.

of the stator winding, which is required to maximize the mutual coupling between stator and field windings, also results in a large inductance. Air-core machines typically have lower power factors than iron-core machines. Further, the field winding of an iron-core machine can be overexcited and controlled to provide power factor compensation, with the result that unity or even leading power factors can be achieved.

Methodology

Table 27 summarizes the pertinent assumptions and considerations for the model. The key to analyzing electromechanical devices is to set the electrical power equal to the mechanical power at the air gap. Figure 36 identifies the basic modeling equations used to determine the values of electrical and magnetic parameters required to meet specific thrust-speed conditions. The phasor diagram shown in Figure 37 defines the terminal conditions for determining the components of electrical power for specific thrust-speed conditions of the LSM.

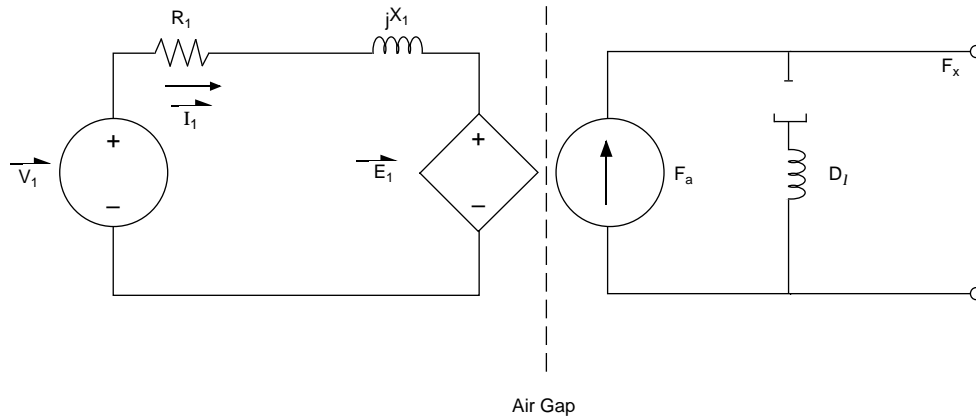
Figure 38 illustrates the joining of the LSM model to a model of the wayside power distribution system to form the model LSMPOWER. The vehicle is shown as a moving wedge of magnetic length l_v . The magnetic length of the vehicle is the

Table 27. LSM model description.

Based on classical synchronous motor models
• Two-axis theory model for iron-core LSMs
• Magnetic coupling model for air-core LSMs
Basic assumptions
• Linear behavior of the magnetic field
• Effects of harmonics not critical to performance
Basic modeling equation at the air gap sets the electrical power equal to the mechanical power
$P_{\text{electrical}} = P_{\text{mechanical}}$
$N_p \cdot E_1 \cdot I_1 \cdot \cos(\gamma_0) = F_a \cdot u_s$
Single LSM model can be used for both iron-core and air-core LSM modeling equations for maglev performance model.

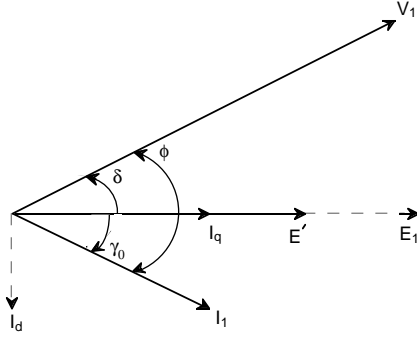
aggregate length of the LSM field windings for each LSM stator on the guideway. For example, in a distributed magnet system, such as the TR07, l_v is the sum of all field magnets on one side of the vehicle. For a bogie system such as Magneplane, l_v is the sum of all of the vehicle-mounted propulsion superconducting coils. The remaining terms of the model are defined on the figure.

LSMPOWER models from the LSMs to the converter stations used to supply conditioned power. That is, it does not model the connection of each system's converter stations to a utility grid (energy



$P_{\text{electrical}} = P_{\text{mechanical}}$	P : Power	γ_0 : Angle between E_1 and I_1
$N_p \cdot E_1 \cdot I_1 \cdot \cos(\gamma_0) = F_a \cdot u_s$	V_1 : Stator voltage	τ_p : Field winding pole pitch
$E_1 = \sqrt{2} \cdot l \cdot p \cdot N \cdot B_1 \cdot u_s$	N_p : Number of phases	D_1 : Mechanical losses
$B_1 = (\pi/2) \cdot [\Phi / (\tau_p \cdot l)]$	F_a : Air gap thrust	I_1 : Stator current
$\Phi = M_f \cdot I_f / p$	F_x : Output thrust	R_1 : Stator resistance
$f_1 = u_s / (2 \cdot \tau_p)$	u_s : Vehicle velocity	X_1 : Stator reactance
	B_1 : Air gap flux density	E_1 : Back EMF
	Φ : Air gap flux	f_1 : Frequency
	l : Stator width	M_f : Mutual inductance
	p : Field pole pairs	I_f : Field current
	N : Turns/pole/phase (or no. of slots/pole/phase)	

Figure 36. LSM equivalent circuit.



At the terminals of the LSM: $\vec{V}_1 = \vec{I}_1 \cdot (R_1 + jX_1) + \vec{E}'$

The output power is given by:

$$\text{Real power} \quad P = N_p \cdot V_1 \cdot I_1 \cdot \cos(\phi)$$

$$\text{Reactive power} \quad Q = N_p \cdot V_1 \cdot I_1 \cdot \sin(\phi)$$

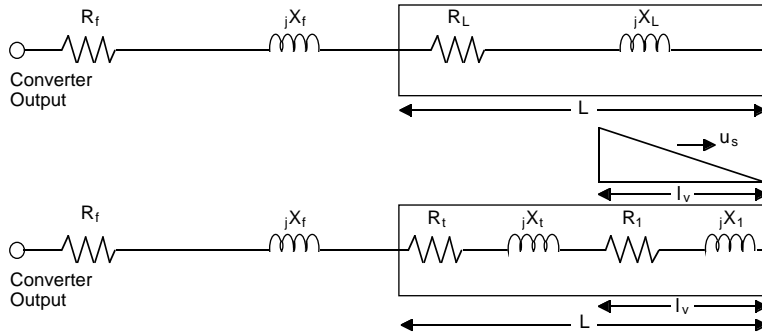
$$\text{Complex power} \quad S = N_p \cdot V_1 \cdot I_1$$

In terms of the power angle (δ):

$$\text{Real power} \quad P = N_p \cdot [V_1 \cdot I_d \cdot \sin(\delta) + V_1 \cdot I_q \cdot \cos(\delta)]$$

Where I_d and I_q are the component phasors of I_1

Figure 37. LSM power output relationships.



L : LSM block length

l_v : Magnetic length of vehicle

R_f : Feeder cable resistance

L_f : Feeder cable inductance ($X_f = 2\pi f L_f$)

R_L : LSM block length resistance

L_L : LSM block length inductance ($X_L = 2\pi f L_L$)

R_t : $R_t = R_L \cdot [(L-l_v)/L]$

L_t : $L_t = L_L \cdot [(L-l_v)/L]$ ($X_t = 2\pi f L_t$)

X : Reactance

f : Frequency

Figure 38. LSM and power system model.

source). We did this to highlight differences attributable to the LSMs. Thus, most of the results here for energy consumption and power factor are at the output of the converter stations. Nevertheless, we separately computed efficiencies and power

factors for these converter stations, and we present resulting overall values for each system in the last subsection here.

Model verification

We used information from Terman (1943), Fitzgerald et al. (1971), Brown and Hamilton (1984), Friedrich et al. (1986), Nasar and Boldea (1987), Miller (1987), and Heinrich and Kretzschmar (1989) to develop and verify the model. In particular, Miller (1987) provided speed-thrust and power data for TR06-II. This earlier vehicle has a similar shape to TR07 and should closely approximate its performance. We, therefore, used the TR06-II data to verify LSMPOWER. We also compared the model's results to those generated by the SCD contractors. In general, agreement was excellent, giving us high confidence in our results.

Application of LSMPOWER to the TR07

Published references could not be obtained that define the thrust-speed requirement for the TR07. However, because of the pending application of TR07 in Florida, private data on several TR07 systems were given to the Government to aid in evaluation. TR07 LSM propulsion-performance data have been released to the GMSA team for their inclusion in this report.

We used the configuration of the Emsland test track power system and frequency converter capacity to estimate the thrust-speed capability of the TR07. The motor current limit of 1200 A per LSM establishes the maximum thrust capability and the frequency converter output transformer ratings of 7.2 MVA per LSM limit the maximum power capability (Heinrich and Kretzschmar 1989). The Transrapid system intended for Florida is expected to have the same 1200-A limit per LSM, but the power capacity of the converter stations is unknown at this time.

Using the LSMPOWER model, we produced performance data for the TR07 operating under the above conditions. The baseline vehicle assumed was a two-car consist. The following parametric data were developed for the analysis:

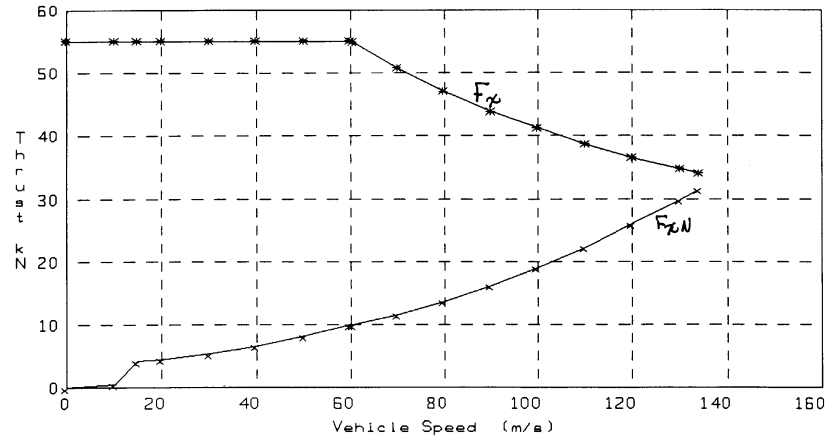
Blocklength resistance R_L :	0.1209 Ω
Blocklength inductance L_L :	0.0005236 H
Direct axis inductance L_{dm} :	0.0002274 H
Quadrature axis inductance L_{qm} :	0.0000944 H
Vehicle magnetic length l_v :	45 m
Longitudinal length of stator L :	300 m
Field winding pole pitch t_p :	0.258 m
Width of LSM stator l :	0.16 m
Pole pairs per LSM p :	75
Slots per pole per phase N :	1
Number of phases N_p :	3
Number of LSMs per consist N_m :	2
Resistance of feeder cable R_f :	0.3 Ω
Inductance of feeder cable L_f :	0.0006 H
Air gap flux density B_l :	0.959 T
Maximum stator current per LSM:	1200 A
Maximum power per LSM:	7.2 MVA

The above data were obtained from available references (Heinrich and Kretzschmar 1989, Friedrich et al. 1986, p. 243–249) and, where possible, were independently verified through calculation.

Figure 39 summarizes the performance capability of the TR07 LSM. The maximum thrust capability of TR07 was determined as 55.1 kN per LSM or 110.2 kN for the consist. Because of the

power limit, the LSM switches from constant thrust to constant power at some speed condition. For the data analyzed, constant thrust changed to constant power at approximately 60 m/s. From this speed to the maximum speed of 133.3 m/s, the power was held constant at the 7.2 MVA per LSM. Thrust and related power, voltages, and current data are shown in Figure 39 for three locations, namely, the input to the active LSM at the vehicle, the input to the LSM stator blocklength, and the output of the frequency converter stations.

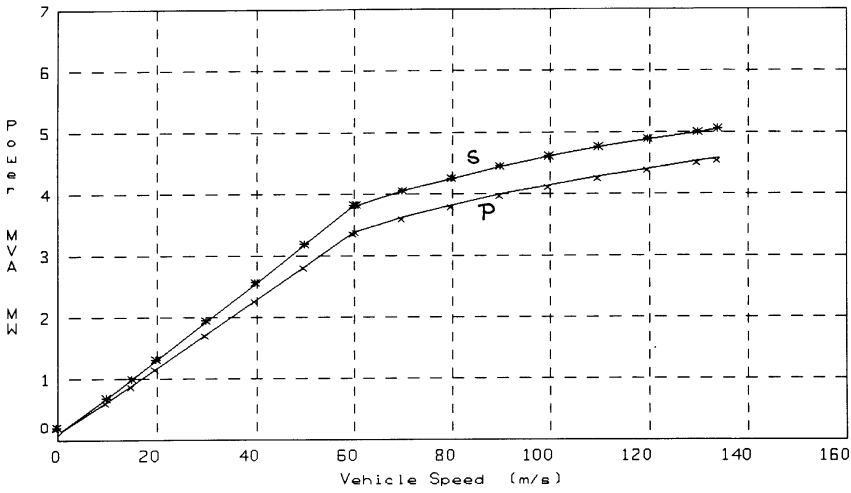
The efficiency of the LSM at maximum thrust capability varies considerably, depending on the measurement location. For example, the efficiency peaks at 99% at the input to the active LSM and is fairly constant over a wide speed range. At the frequency converter output, the efficiency peaks at 87% at a speed of 133.3 m/s. The efficiency at this point is also quite sensitive to speed because of the power losses in the feeder cable and LSM blocklength. The power factor shows similar trends, with it being approximately 90% lagging at the active input to the LSM and approximately



U_s (m/s)	F_x (kN)	F_{xN} (kN)	E_1 (V)	V_1 (V)	I_1 (A)	P (MW)	S (MVA)	PF (PU)	E_{fg} (PU)
0.0	55.1	0.0	0	22	1201	.08	.08	1.00	0.00
10.0	55.1	0.5	163	193	1201	.63	.69	.91	.88
15.0	55.1	4.1	244	279	1201	.90	1.01	.90	.91
20.0	55.1	4.5	326	366	1201	1.18	1.32	.90	.93
30.0	55.1	5.4	488	539	1201	1.73	1.94	.89	.95
40.0	55.1	6.6	651	712	1201	2.28	2.56	.89	.97
50.0	55.1	8.1	814	885	1201	2.83	3.19	.89	.97
60.0	55.1	9.9	977	1058	1201	3.38	3.81	.89	.98
60.5	54.9	10.0	985	1066	1196	3.40	3.82	.89	.98
70.0	50.7	11.6	1140	1223	1105	3.62	4.05	.89	.98
80.0	47.0	13.7	1302	1388	1024	3.82	4.26	.90	.99
90.0	43.8	16.2	1465	1552	955	3.99	4.45	.90	.99
100.0	41.1	19.1	1628	1716	895	4.15	4.61	.90	.99
110.0	38.7	22.3	1791	1880	843	4.29	4.76	.90	.99
120.0	36.6	25.9	1954	2044	797	4.42	4.89	.91	.99
130.0	34.7	29.8	2116	2208	756	4.54	5.01	.91	.99
134.0	34.0	31.5	2182	2274	741	4.59	5.05	.91	.99

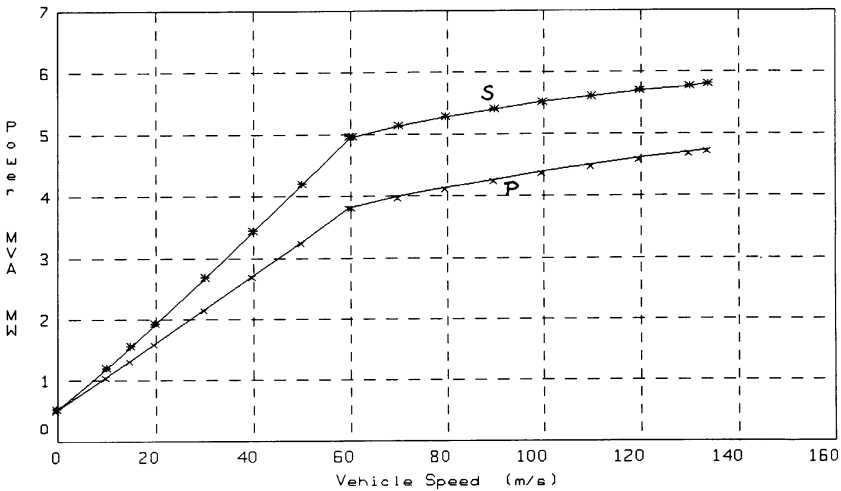
a. LSM thrust vs. speed, maximum thrust.

Figure 39. Performance capability of the TR07 LSM.



b. LSM power vs. speed, maximum thrust.

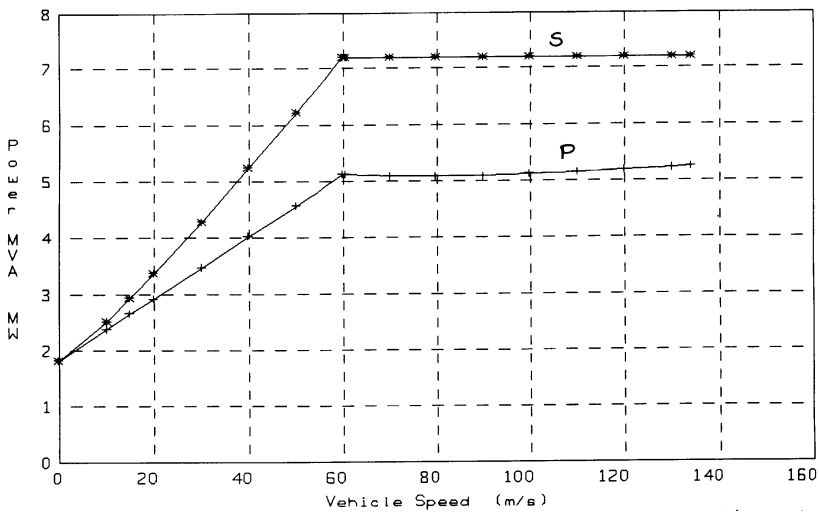
U_s (m/s)	F_x (kN)	F_{xN} (kN)	E_1 (V)	V_1 (V)	I_1 (A)	P (MW)	S (MVA)	PF (PU)	E_{eff} (PU)
0.0	55.1	0.0	0	22	1201	.08	.08	1.00	0.00
10.0	55.1	0.5	163	193	1201	.63	.69	.91	.88
15.0	55.1	4.1	244	279	1201	.90	1.01	.90	.91
20.0	55.1	4.5	326	366	1201	1.18	1.32	.90	.93
30.0	55.1	5.4	488	539	1201	1.73	1.94	.89	.95
40.0	55.1	6.6	651	712	1201	2.28	2.56	.89	.97
50.0	55.1	8.1	814	885	1201	2.83	3.19	.89	.97
60.0	55.1	9.9	977	1058	1201	3.38	3.81	.89	.98
60.5	54.9	10.0	985	1066	1196	3.40	3.82	.89	.98
70.0	50.7	11.6	1140	1223	1105	3.62	4.05	.89	.98
80.0	47.0	13.7	1302	1388	1024	3.82	4.26	.90	.99
90.0	43.8	16.2	1465	1552	955	3.99	4.45	.90	.99
100.0	41.1	19.1	1628	1716	895	4.15	4.61	.90	.99
110.0	38.7	22.3	1791	1880	843	4.29	4.76	.90	.99
120.0	36.6	25.9	1954	2044	797	4.42	4.89	.91	.99
130.0	34.7	29.8	2116	2208	756	4.54	5.01	.91	.99
134.0	34.0	31.5	2182	2274	741	4.59	5.05	.91	.99



c. Blocklength input power, maximum thrust.

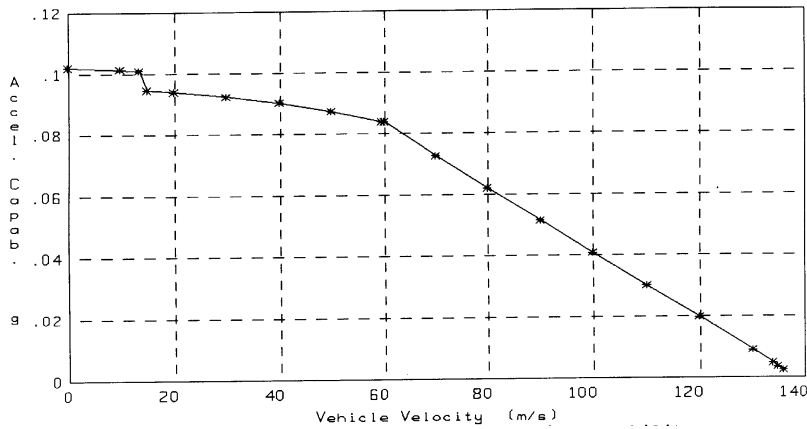
U_s (m/s)	F_x (kN)	F_{xN} (kN)	E_1 (V)	V_L (V)	I_1 (A)	PL (MW)	SL (MVA)	PF (PU)	E_{eff} (PU)
0.0	55.1	0.0	0	145	1201	.52	.52	1.00	0.00
10.0	55.1	0.5	163	332	1201	1.07	1.20	.90	.51
15.0	55.1	4.1	244	434	1201	1.35	1.56	.86	.61
20.0	55.1	4.5	326	537	1201	1.62	1.94	.84	.68
30.0	55.1	5.4	488	746	1201	2.18	2.69	.81	.76
40.0	55.1	6.6	651	956	1201	2.73	3.44	.79	.81
50.0	55.1	8.1	814	1167	1201	3.28	4.20	.78	.84
60.0	55.1	9.9	977	1378	1201	3.83	4.96	.77	.86
60.5	54.9	10.0	985	1386	1196	3.84	4.97	.77	.86
70.0	50.7	11.6	1140	1548	1105	3.99	5.13	.78	.89
80.0	47.0	13.7	1302	1716	1024	4.14	5.27	.79	.91
90.0	43.8	16.2	1465	1883	955	4.27	5.39	.79	.92
100.0	41.1	19.1	1628	2049	895	4.40	5.50	.80	.93
110.0	38.7	22.3	1791	2214	843	4.51	5.60	.81	.94
120.0	36.6	25.9	1954	2379	797	4.62	5.69	.81	.95
130.0	34.7	29.8	2116	2543	756	4.72	5.77	.82	.96
134.0	34.0	31.5	2182	2609	741	4.75	5.80	.82	.96

Figure 39 (cont'd). Performance capability of the TR07 LSM.



d. Converter station output power, maximum thrust.

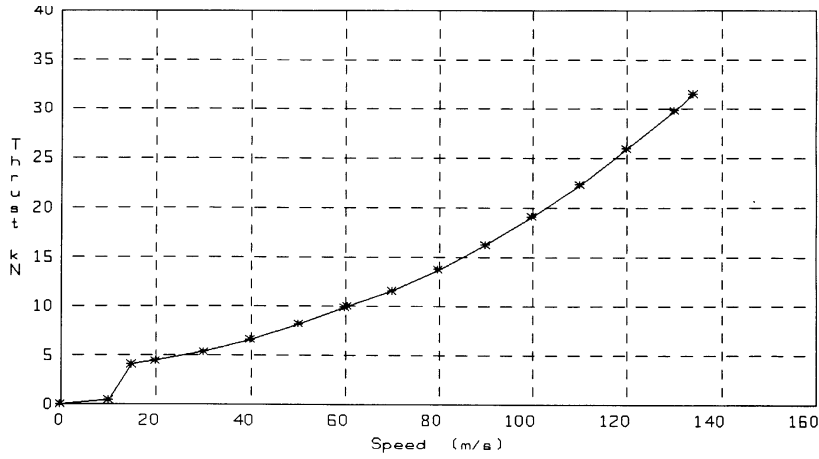
U_s (m/s)	F_x (kN)	F_{xN} (kN)	V_s (V)	I_s (V)	P_s (MW)	S_s (MVA)	PF (PU)	E_{sc} (PU)
0.0	55.1	0.0	505	1201	1.82	1.82	1.00	0.00
10.0	55.1	0.5	699	1201	2.37	2.52	.94	.23
15.0	55.1	4.1	814	1201	2.65	2.93	.90	.31
20.0	55.1	4.5	936	1201	2.92	3.37	.87	.38
30.0	55.1	5.4	1192	1201	3.47	4.29	.81	.48
40.0	55.1	6.6	1457	1201	4.02	5.25	.77	.55
50.0	55.1	8.1	1726	1201	4.58	6.22	.74	.60
60.0	55.1	9.9	1998	1201	5.13	7.20	.71	.64
60.5	54.9	10.0	2007	1196	5.13	7.20	.71	.65
70.0	50.7	11.6	2173	1105	5.09	7.20	.71	.70
80.0	47.0	13.7	2344	1024	5.08	7.20	.71	.74
90.0	43.8	16.2	2513	955	5.09	7.20	.71	.77
100.0	41.1	19.1	2681	895	5.12	7.20	.71	.80
110.0	38.7	22.3	2847	843	5.15	7.20	.72	.83
120.0	36.6	25.9	3011	797	5.19	7.20	.72	.85
130.0	34.7	29.8	3175	756	5.23	7.20	.73	.86
134.0	34.0	31.5	3240	741	5.25	7.20	.73	.87



e. Acceleration capability, maximum thrust.

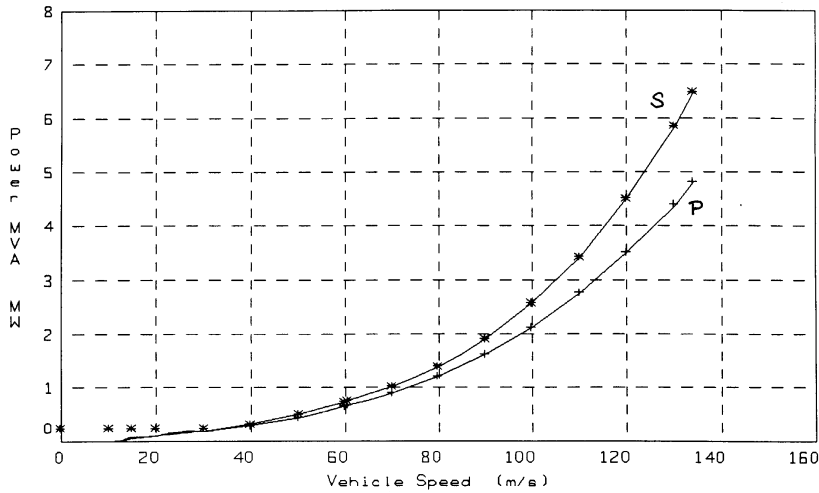
U_s (m/s)	F_x (kN)	F_{xN} (kN)	Accel (g)	Accel (m/s ²)
0.0	55.1	0.0	0.102	1.001
10.0	55.1	0.4	0.101	0.994
13.4	55.1	0.6	0.101	0.990
15.0	55.1	4.1	0.095	0.927
20.0	55.1	4.4	0.094	0.920
30.0	55.1	5.4	0.092	0.904
40.0	55.1	6.6	0.090	0.882
50.0	55.1	8.1	0.087	0.854
59.7	55.1	9.9	0.084	0.822
60.1	55.1	9.9	0.084	0.821
70.0	50.7	11.6	0.073	0.712
80.0	47.0	13.7	0.062	0.606
90.0	43.8	16.2	0.051	0.502
100.0	41.1	19.1	0.041	0.400
110.0	38.7	22.3	0.030	0.298
120.0	36.6	25.9	0.020	0.194
130.0	34.7	29.8	0.009	0.088
134.0	34.0	31.5	0.005	0.045
135.0	33.8	31.9	0.003	0.034

Figure 39 (cont'd).



f. LSM thrust vs. speed, normal thrust.

U _s (m/s)	F _x (kN)	E ₁ (V)	V ₁ (V)	I ₁ (A)	P (MW)	S (MVA)	PF (PU)	E _{eff} (PU)
0.0	0.0	0.0	0.0	0.0	0.00	0.00	.94	1.00
10.0	0.5	162.8	163.1	10.9	.01	.01	.94	1.00
15.0	4.1	244.2	246.7	89.4	.06	.07	.94	.99
20.0	4.5	325.6	328.7	97.0	.09	.10	.94	.99
30.0	5.4	488.4	492.9	116.8	.16	.17	.94	1.00
40.0	6.6	651.2	657.9	143.4	.26	.28	.93	1.00
50.0	8.1	814.0	823.5	176.7	.41	.44	.93	1.00
60.0	9.9	976.8	990.1	215.4	.60	.64	.93	1.00
60.5	10.0	984.9	998.4	216.9	.60	.65	.93	1.00
70.0	11.6	1139.6	1157.1	252.0	.81	.87	.93	1.00
80.0	13.7	1302.4	1325.4	298.1	1.10	1.19	.93	1.00
90.0	16.2	1465.2	1495.3	352.9	1.46	1.58	.93	1.00
100.0	19.1	1628.0	1666.9	415.7	1.92	2.08	.92	1.00
110.0	22.3	1790.8	1840.5	486.3	2.47	2.69	.92	.99
120.0	25.9	1953.6	2016.2	564.7	3.13	3.42	.92	.99
130.0	29.8	2116.4	2194.4	650.3	3.90	4.28	.91	.99
134.0	31.5	2181.5	2266.5	686.7	4.25	4.67	.91	.99



g. Converter station output power, normal thrust.

U _s (m/s)	F _x (kN)	V _s (V)	I _s (A)	P _s (MW)	S _s (MVA)	PF (PU)	E _{eff} (PU)
0.0	0.0	0.0	0.0	0.00	0.00	.94	1.00
10.0	0.5	167.7	10.9	.01	.01	.94	.97
15.0	4.1	286.4	89.4	.07	.08	.93	.86
20.0	4.5	374.0	97.0	.10	.11	.93	.88
30.0	5.4	553.3	116.8	.18	.19	.92	.90
40.0	6.6	739.4	143.4	.29	.32	.91	.91
50.0	8.1	933.8	176.7	.44	.50	.90	.91
60.0	9.9	1137.4	215.4	.65	.73	.89	.91
60.5	10.0	1147.4	216.9	.66	.75	.89	.91
70.0	11.6	1345.2	252.0	.89	1.02	.87	.91
80.0	13.7	1568.2	298.1	1.21	1.40	.86	.91
90.0	16.2	1808.8	352.9	1.61	1.91	.84	.90
100.0	19.1	2069.6	415.7	2.13	2.58	.82	.90
110.0	22.3	2353.6	486.3	2.75	3.43	.80	.89
120.0	25.9	2664.3	564.7	3.51	4.51	.78	.89
130.0	29.8	3005.0	650.3	4.41	5.86	.75	.88
134.0	31.5	3150.6	686.7	4.82	6.49	.74	.88

Figure 39 (cont'd). Performance capability of the TR07 LSM.

72% lagging at the frequency converter output. The low power factor at the converter output location is heavily influenced by the reactance of the feeder cable.

The results of the LSMPOWER analysis for the TR07 compare well with the limited published data and the private data available to the Government.

Application of LSMPOWER to the SCD linear synchronous motors

Grumman. The Grumman LSM concept provides integrated levitation, guidance, and propulsion with a single machine. It has an iron-core LSM with a conventional stator. Like the TR07, there are two LSMs per vehicle. The levitation magnets are distributed over the length of the vehicle, and these magnets use superconducting coils in conjunction with iron cores. Conventional control coils on the magnets are used for levitation, and the combination of superconducting coils with conventional control coils achieves an air gap of 40 mm.

The LSM blocklengths are typically 1000 m and are center-fed in 500-m segments. Converter station blocklengths are 4000 m with cables feeding each 1000-m block. The LSM field current is set for operation at a leading power factor, with the intent of achieving a power factor that is close to unity at the input to the LSM block.

Linear generator coils are set into the field winding pole faces in a way similar to the TR07 to transfer power to the vehicle. In addition to these coils, high-frequency power is injected into the LSM stator coils and transferred to the vehicle via a transformer. These two techniques, when taken together, provide all-speed power transfer capability to the Grumman SCD vehicle; this concept does not require the auxiliary batteries of the TR07.

We produced performance data using the LSMPOWER model for the Grumman SCD operating as described above. The baseline vehicle was assumed to be a two-car consist. Grumman's baseline concept also makes use of an aluminum LSM winding, which produces a maximum thrust of 30 kN per LSM. This results in a low-speed acceleration capability of only 0.09 g. For better acceleration and grade-climbing capability, the Grumman LSM would have to be modified by replacing the aluminum LSM stator winding with a copper winding.

We used the following parametric data, determined from the baseline case of aluminum stator windings, in our analysis:

Blocklength resistance R_L :	0.1772 Ω
Blocklength inductance L_L :	0.0012 H
Direct axis inductance L_{dm} :	0.00005 H
Quadrature axis inductance L_{qm} :	0.00003 H
Vehicle magnetic length l_v :	18 m
Longitudinal length of stator L :	500 m
Field winding pole pitch t_p :	0.75 m
Width of LSM stator l :	0.20 m
Pole pairs per LSM p :	12
Slots per pole per phase N :	3
Number of phases N_p :	3
Number of LSMs per consist N_m :	2
Resistance of feeder cable R_f :	0.139 Ω
Inductance of feeder cable L_f :	0.0012 H
Air gap flux density B_1 :	0.896 T
Maximum stator current per LSM:	1343 A
Maximum power per LSM:	7.5 MVA

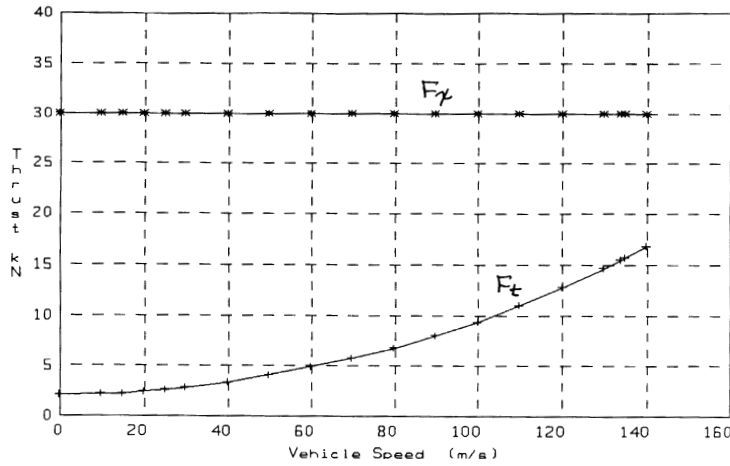
The above data were obtained from information provided by Grumman during the in-progress reviews (IPRs) and from the SCD final report (Grumman 1992a), and, where possible, were independently verified through calculation.

Figure 40 summarizes the performance capability of the Grumman SCD LSM. The maximum thrust capability of Grumman's two-car consist is 30 kN per LSM or 60 kN for the consist. The design provides a constant thrust up to the design speed of 134 m/s. The charts in these figures show thrust and related power, voltages, and current data for two locations, namely, the input to the active LSM at the vehicle and the output of the frequency converter stations. Data are shown for both maximum- and nominal-thrust conditions. The power-limited condition of 7.5 MVA per LSM is just reached at 134 m/s.

Figure 40e shows the acceleration capability for the baseline 61,224-kg vehicle. With a total thrust of 60 kN, the LSM may maintain a maximum vehicle acceleration of about 0.09 g from zero speed to 60 m/s; this diminishes to 0.05 g at 134 m/s.

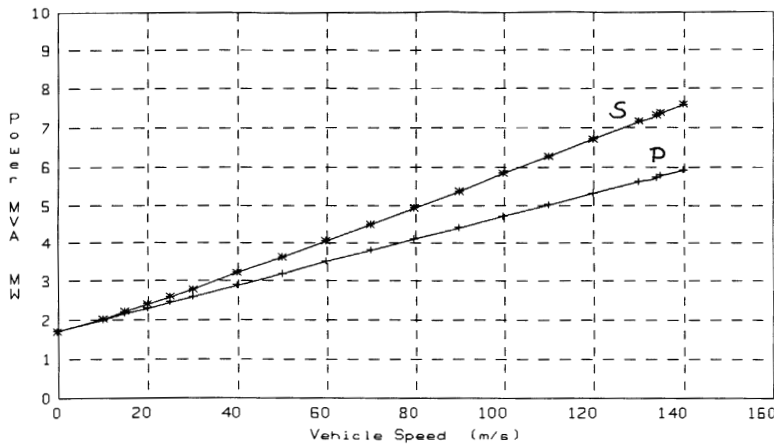
Grumman also developed the parameters for an LSM with a copper stator winding. This motor has a maximum thrust of 100 kN. It has a low-speed acceleration capability of about 0.16 g and has reserve acceleration of about 0.09 g at 134 m/s. Figure 40f shows the acceleration vs. speed capability of this 100-kN LSM.

The efficiency of the LSM at maximum thrust varies considerably, depending on the measurement location. For example, the efficiency peaks at 99% at the input to the active LSM and is fairly constant over a wide speed range. At the frequency converter output, the efficiency peaks at 70% at a speed of 134 m/s. The efficiency at this location is also quite sensitive to speed because



a. LSM thrust vs. speed, maximum thrust.

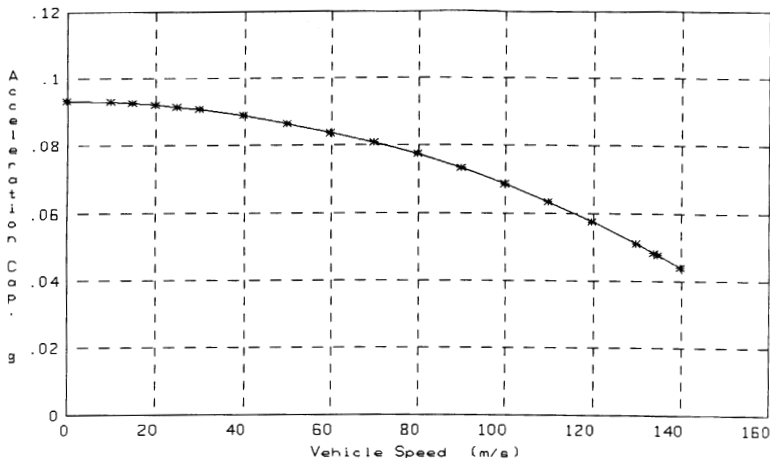
U_s (m/s)	F_x (kN)	F_t (kN)	E_1 (V)	V_1 (V)	I_1 (A)	P (MW)	S (MVA)	Q (MVAR)	PF (PU)	E_{eff} (PU)
0.0	30.0	2.05	0.0	8.6	1343.0	0.03	0.03	0.00	1.000	0.000
10.0	30.0	2.13	91.2	96.3	1343.0	0.33	0.39	-0.20	0.863	0.897
15.0	30.0	2.23	136.9	140.7	1343.0	0.48	0.57	-0.29	0.855	0.929
20.0	30.0	2.37	182.5	185.2	1343.0	0.63	0.75	-0.39	0.850	0.946
25.0	30.0	2.55	228.1	229.7	1343.0	0.78	0.93	-0.49	0.848	0.956
30.0	30.0	2.77	273.7	274.1	1343.0	0.93	1.10	-0.59	0.846	0.963
40.0	30.0	3.33	364.9	363.1	1343.0	1.23	1.46	-0.79	0.844	0.972
50.0	30.0	4.05	456.2	452.1	1343.0	1.53	1.82	-0.98	0.842	0.978
60.0	30.0	4.93	547.4	541.1	1343.0	1.83	2.18	-1.18	0.842	0.981
70.0	30.0	5.75	638.6	630.0	1343.0	2.13	2.54	-1.37	0.841	0.984
80.0	30.0	6.77	729.9	719.0	1343.0	2.43	2.90	-1.57	0.840	0.986
90.0	30.0	7.99	821.1	808.0	1343.0	2.73	3.26	-1.77	0.840	0.987
100.0	30.0	9.40	912.3	897.0	1343.0	3.03	3.61	-1.96	0.840	0.989
110.0	30.0	10.99	1003.6	985.9	1343.0	3.33	3.97	-2.16	0.839	0.990
120.0	30.0	12.76	1094.8	1074.9	1343.0	3.63	4.33	-2.36	0.839	0.991
130.0	30.0	14.69	1186.0	1163.9	1343.0	3.93	4.69	-2.55	0.839	0.991
134.0	30.0	15.52	1222.5	1199.5	1343.0	4.05	4.83	-2.63	0.839	0.991
135.0	30.0	15.72	1231.7	1208.4	1343.0	4.08	4.87	-2.65	0.839	0.992



b. Converter station output power, maximum thrust.

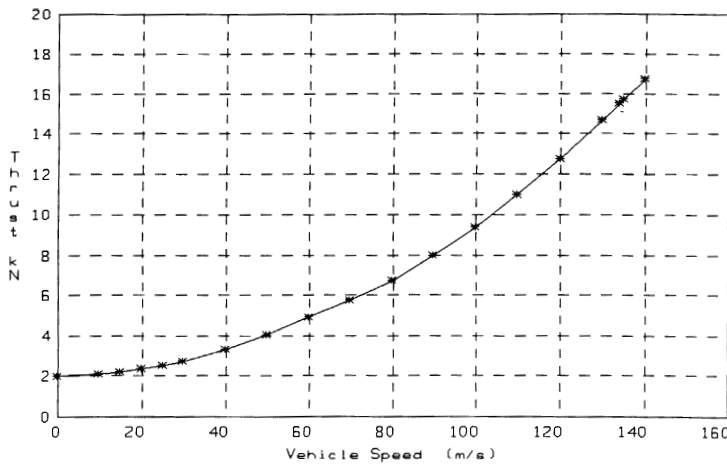
U_s (m/s)	F_x (kN)	F_t (kN)	V_s (V)	I_s (A)	P (MW)	S (MVA)	Q (MVAR)	PF (PU)	E_{eff} (PU)
0.0	30.0	2.05	424.7	1343.0	1.711	1.711	0.000	1.000	0.000
10.0	30.0	2.13	506.2	1343.0	2.011	2.040	0.341	0.986	0.149
15.0	30.0	2.23	551.1	1343.0	2.161	2.221	0.511	0.973	0.208
20.0	30.0	2.37	598.0	1343.0	2.311	2.409	0.682	0.959	0.260
25.0	30.0	2.55	646.4	1343.0	2.461	2.604	0.852	0.945	0.305
30.0	30.0	2.77	695.9	1343.0	2.611	2.804	1.022	0.931	0.345
40.0	30.0	3.33	797.8	1343.0	2.911	3.214	1.363	0.906	0.412
50.0	30.0	4.05	902.2	1343.0	3.211	3.635	1.704	0.883	0.467
60.0	30.0	4.93	1008.4	1343.0	3.511	4.063	2.045	0.864	0.513
70.0	30.0	5.75	1115.9	1343.0	3.811	4.496	2.385	0.848	0.551
80.0	30.0	6.77	1224.3	1343.0	4.111	4.933	2.726	0.833	0.584
90.0	30.0	7.99	1333.4	1343.0	4.411	5.372	3.067	0.821	0.612
100.0	30.0	9.40	1443.1	1343.0	4.711	5.814	3.408	0.810	0.637
110.0	30.0	10.99	1553.2	1343.0	5.011	6.258	3.748	0.801	0.659
120.0	30.0	12.76	1663.6	1343.0	5.311	6.703	4.089	0.792	0.678
130.0	30.0	14.69	1774.3	1343.0	5.611	7.149	4.430	0.785	0.695
134.0	30.0	15.52	1818.7	1343.0	5.731	7.328	4.566	0.782	0.701
135.0	30.0	15.72	1829.8	1343.0	5.761	7.372	4.600	0.781	0.703

Figure 40. Performance capability of the Grumman SCD LSM.



U_s (m/s)	F_x (kN)	F_L (kN)	Accel (g)	Accel (m/s ²)
0.0	30.0	2.05	0.093	0.913
10.0	30.0	2.13	0.093	0.910
15.0	30.0	2.23	0.093	0.907
20.0	30.0	2.37	0.092	0.903
25.0	30.0	2.55	0.091	0.897
30.0	30.0	2.77	0.091	0.890
40.0	30.0	3.33	0.089	0.871
50.0	30.0	4.05	0.086	0.848
60.0	30.0	4.93	0.084	0.819
70.0	30.0	5.75	0.081	0.792
80.0	30.0	6.77	0.077	0.759
90.0	30.0	7.99	0.073	0.719
100.0	30.0	9.40	0.069	0.673
110.0	30.0	10.99	0.063	0.621
120.0	30.0	12.76	0.057	0.563
130.0	30.0	14.69	0.051	0.500
134.0	30.0	15.52	0.048	0.473
135.0	30.0	15.72	0.048	0.466

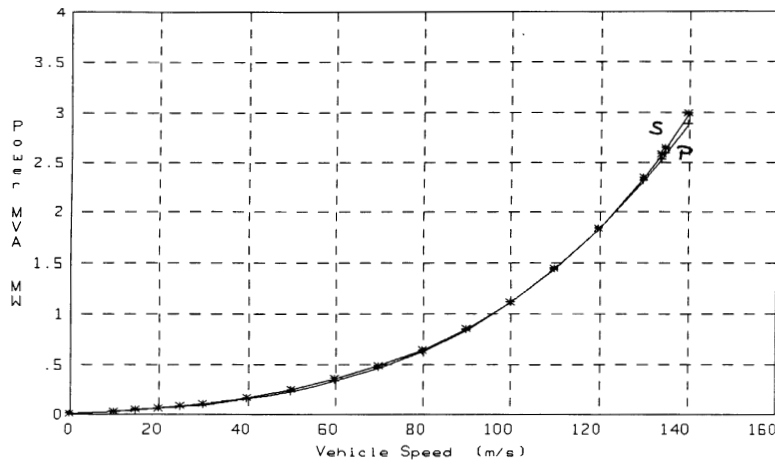
c. Acceleration capability, maximum thrust.



U_s (m/s)	F_x (kN)	E_1 (kN)	V_1 (V)	I_1 (A)	P (MW)	S (MVA)	Q (MVAR)	PF (PU)	E_{zf} (PU)
0.0	2.05	0.0	0.6	91.8	0.00	0.00	0.00	1.000	0.000
10.0	2.13	91.2	91.6	95.4	0.02	0.03	-0.02	0.820	0.992
15.0	2.23	136.9	137.1	99.8	0.03	0.04	-0.02	0.819	0.994
20.0	2.37	182.5	182.7	106.1	0.05	0.06	-0.03	0.819	0.995
25.0	2.55	228.1	228.2	114.2	0.06	0.08	-0.04	0.819	0.996
30.0	2.77	273.7	273.7	124.0	0.08	0.10	-0.06	0.819	0.996
40.0	3.33	364.9	364.7	149.1	0.13	0.16	-0.09	0.819	0.997
50.0	4.05	456.2	455.6	181.3	0.20	0.25	-0.14	0.820	0.997
60.0	4.93	547.4	546.3	220.7	0.30	0.36	-0.21	0.820	0.997
70.0	5.75	638.6	636.9	257.4	0.40	0.49	-0.28	0.821	0.997
80.0	6.77	729.9	727.3	303.1	0.54	0.66	-0.38	0.822	0.997
90.0	7.99	821.1	817.5	357.8	0.72	0.88	-0.50	0.823	0.997
100.0	9.40	912.3	907.3	420.9	0.94	1.15	-0.65	0.824	0.996
110.0	10.99	1003.6	996.9	492.1	1.21	1.47	-0.83	0.825	0.996
120.0	12.76	1094.8	1086.1	571.1	1.54	1.86	-1.05	0.826	0.996
130.0	14.69	1186.0	1175.0	657.8	1.92	2.32	-1.30	0.827	0.996
134.0	15.52	1222.5	1210.4	694.6	2.09	2.52	-1.41	0.828	0.996
135.0	15.72	1231.7	1219.2	704.0	2.13	2.57	-1.44	0.828	0.996

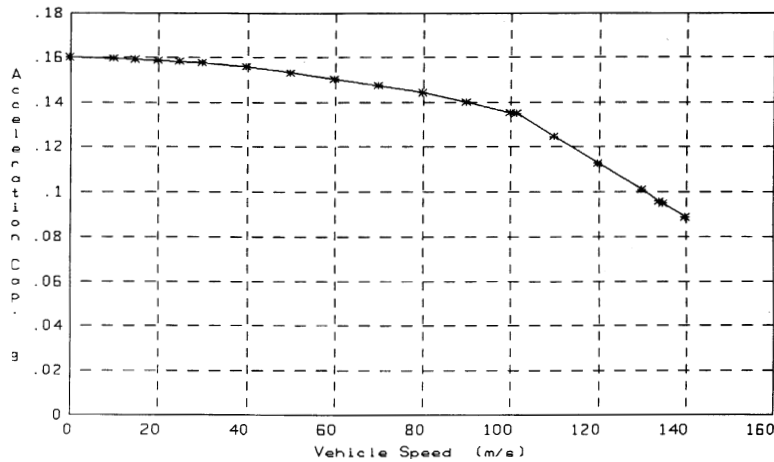
d. LSM thrust vs. speed, normal thrust.

Figure 40 (cont'd).



U_s (m/s)	F_x (kN)	V_s (V)	I_s (A)	P (MW)	S (MVA)	Q (MVAR)	PF (PU)	E_{eff} (PU)
0.0	2.05	29.0	91.8	0.008	0.008	0.000	1.000	0.000
10.0	2.13	113.1	95.4	0.030	0.032	-0.012	0.925	0.712
15.0	2.23	156.8	99.8	0.043	0.047	-0.019	0.914	0.780
20.0	2.37	200.8	106.1	0.058	0.064	-0.027	0.909	0.816
25.0	2.55	244.8	114.2	0.076	0.084	-0.035	0.908	0.838
30.0	2.77	288.8	124.0	0.098	0.107	-0.045	0.909	0.851
40.0	3.33	376.1	149.1	0.154	0.168	-0.067	0.917	0.863
50.0	4.05	462.4	181.3	0.234	0.252	-0.093	0.929	0.867
60.0	4.93	547.3	220.7	0.342	0.362	-0.120	0.944	0.865
70.0	5.75	630.3	257.4	0.465	0.487	-0.143	0.956	0.865
80.0	6.77	713.0	303.1	0.629	0.648	-0.158	0.970	0.861
90.0	7.99	796.6	357.8	0.841	0.855	-0.156	0.983	0.856
100.0	9.40	883.0	420.9	1.108	1.115	-0.122	0.994	0.848
110.0	10.99	975.0	492.1	1.439	1.439	-0.039	1.000	0.840
120.0	12.76	1076.2	571.1	1.840	1.844	0.116	0.998	0.832
130.0	14.69	1191.0	657.8	2.321	2.350	0.373	0.987	0.823
134.0	15.52	1241.8	694.6	2.537	2.588	0.511	0.980	0.820
135.0	15.72	1255.0	704.0	2.593	2.650	0.549	0.978	0.819

e. Converter station output power, normal thrust.



U_s (m/s)	F_x (kN)	F_t (kN)	Accel (g)	Accel (m/s ²)
0.0	50.0	2.05	0.160	1.566
10.0	50.0	2.13	0.159	1.564
15.0	50.0	2.23	0.159	1.560
20.0	50.0	2.37	0.159	1.556
25.0	50.0	2.55	0.158	1.550
30.0	50.0	2.77	0.157	1.543
40.0	50.0	3.33	0.155	1.525
50.0	50.0	4.05	0.153	1.501
60.0	50.0	4.93	0.150	1.472
70.0	50.0	5.75	0.147	1.446
80.0	50.0	6.77	0.144	1.412
90.0	50.0	7.99	0.140	1.372
100.0	50.0	9.40	0.135	1.326
101.6	50.0	9.65	0.134	1.318
110.0	48.3	10.99	0.124	1.220
120.0	46.5	12.76	0.113	1.104
130.0	44.9	14.69	0.101	0.988
134.0	44.4	15.52	0.096	0.942

f. Acceleration capability for 100-kN design, maximum thrust.

Figure 40 (cont'd). Performance capability of the Grumman SCD LSM.

of the power losses in the feeder cable and LSM blocklength.

The power factor shows similar trends: it is approximately 87% leading at the active input to the LSM, is unity as intended at the input the LSM blocklength, and is approximately 80% lagging at the frequency converter output location. The relatively high power factor at this location is the result of the leading power factor, which partly compensates for the reactive power requirements of the feeder cable.

The LSM parameters used by LSMPOWER for the Grumman concept differ somewhat from those specified by Grumman, particularly with respect to the internal phase angle of the machine. LSMPOWER derives these parameters, where in the Grumman model they are apparently specified. However, the LSMPOWER performance results agree fairly closely with those predicted by Grumman. The difference in model parameters appears to be caused by the different modeling approaches taken.

Magneplane. The Magneplane LSM is an air-core machine with a conventional meander winding. The concept uses one LSM per vehicle, with a propulsion winding air gap of approximately 250 mm. Superconducting propulsion coils are located on bogies at each end of the vehicle. The propulsion coil design is intended to minimize the stray fields in the passenger compartment. This is accomplished by operating the inboard superconducting coils at lower field strengths compared to the outboard coils. The LSM thrust control angle is set for zero lift capability for normal operation. This angle is controlled to provide lift from the LSM for heave damping.

The LSM blocklengths are 2000 m for the baseline concept and are end-fed from the converter stations. Converter stations are located at every other blocklength and are assumed to be located close enough to the guideway as to not require feeder cables of any significant length. Here, we include feeder cables in the analysis for comparison with the other concepts.

The LSM stator winding is a high inductance winding, and a power factor correction for each LSM winding is planned. Magneplane did not fully develop the details of the power factor correction; the analysis here considers one preliminary case of power factor correction to estimate its effect.

For obtaining vehicle power, the LSM windings will be used as the primary of an air-core transformer. The LSM interacts with an 18-m coil that

is located under the vehicle and between the two bogies. High-frequency power is injected into the LSM stator winding and transferred to the vehicle via the air-core transformer.

We produced the following performance data using the LSMPOWER model for the Magneplane SCD operating as described above. The baseline vehicle was a one-car consist.

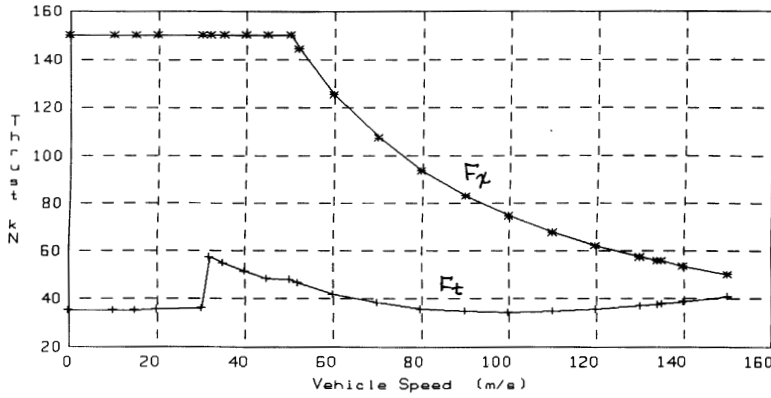
Blocklength resistance R_L :	0.20 Ω
Blocklength inductance L_L :	0.0142 H
Vehicle magnetic length l_v :	2000 m
Longitudinal length of stator L :	2000 m
Field winding pole pitch t_p :	0.75 m
Width of LSM stator l :	1.2 m
Pole pairs per LSM p :	2
Slots per pole per phase N :	4
Number of phases N_p :	3
Number of LSMs per consist N_m :	1
Resistance of feeder cable R_f :	0.139 Ω
Inductance of feeder cable L_f :	0.0012 H
Back EMF characteristic at a specified speed E_f :	2326 V at 150 m/s
Maximum stator current per LSM:	3224 A
Maximum mechanical power output:	7.5 MW for vehicle

The above data were obtained from information provided by Magneplane during the IPRs and from their SCD final report (Magneplane 1992a), and where possible were independently verified through calculation. These data show the magnetic length of the vehicle being the same as the LSM blocklength to account for the equivalent circuit parameters as specified by Magneplane.

Figure 41 summarizes the performance capability of the Magneplane SCD LSM. The Magneplane design requires nearly constant thrust at all speeds, primarily because of the high magnetic drag at low speeds and the high aerodynamic drag at high speeds. The magnetic drag peaks in the vicinity of 20–40 m/s. The maximum thrust capability of the one-car consist was 150 kN. Thrust and related power, voltages, and current data are shown in the following charts for two locations, namely, the input to the LSM blocklength and the output of the frequency converter station.

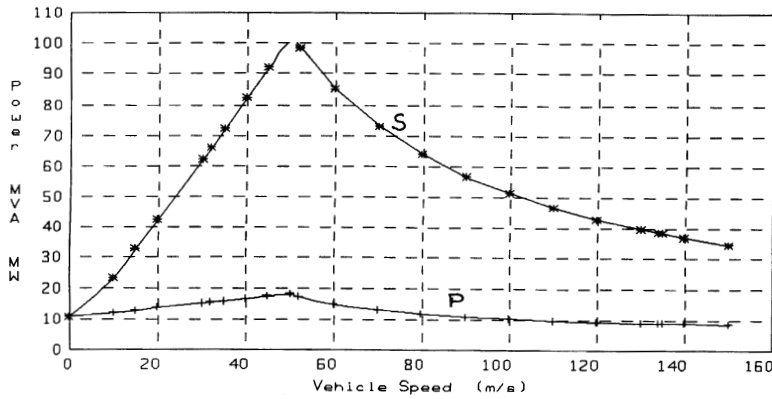
The thrust-speed breakpoint from constant thrust to constant power occurs at 50 m/s. The very high megavolt-ampere requirement at this point, 94 MVA compared to 14 MW of active power, was a result of the very high inductance of the stator winding without any capacitive compensation. The power factor correction planned by Magneplane should take care of this problem.

Figures 41e and f show preliminary estimates of the reduced megavolt-ampere requirement



U_s (m/s)	F_x (kN)	P_x (MW)	F_t (kN)	E_1 (V)	V_1 (V)	I_1 (A)	P (MW)	S (MVA)	PF (PU)	E_{ff} (PU)
0.0	150.0	0.00	35.08	0.0	644.9	3224.	6.24	6.24	1.000	0.000
10.0	150.0	1.50	35.18	155.1	2078.1	3224.	7.74	20.10	0.385	0.194
15.0	150.0	2.25	35.32	232.6	3007.7	3224.	8.49	29.09	0.292	0.265
20.0	150.0	3.00	35.50	310.1	3952.9	3224.	9.24	38.24	0.242	0.325
30.0	150.0	4.50	36.04	465.2	5859.8	3224.	10.74	56.68	0.189	0.419
32.0	150.0	4.80	36.04	496.2	6242.5	3224.	11.04	60.39	0.183	0.435
35.0	150.0	5.25	35.92	542.7	6816.9	3224.	11.49	65.94	0.174	0.457
40.0	150.0	6.00	35.37	620.3	7775.3	3224.	12.24	75.21	0.163	0.490
45.0	150.0	6.75	34.34	697.8	8734.4	3224.	12.99	84.49	0.154	0.520
50.0	150.0	7.50	33.90	775.3	9694.2	3224.	13.74	93.77	0.147	0.546
52.0	144.2	7.50	34.46	806.3	9695.1	3100.	13.27	90.18	0.147	0.565
60.0	125.0	7.50	31.87	930.4	9701.2	2687.	11.83	78.20	0.151	0.634
70.0	107.1	7.50	28.14	1085.5	9713.4	2303.	10.68	67.11	0.159	0.702
80.0	93.8	7.50	25.91	1240.5	9729.4	2015.	9.94	58.82	0.169	0.755
90.0	83.3	7.50	24.76	1395.6	9748.6	1791.	9.43	52.39	0.180	0.796
100.0	75.0	7.50	24.42	1550.7	9770.8	1612.	9.06	47.26	0.192	0.828
110.0	68.2	7.50	24.74	1705.7	9795.7	1466.	8.79	43.07	0.204	0.853
120.0	62.5	7.50	25.61	1860.8	9823.2	1344.	8.58	39.59	0.217	0.874
130.0	57.7	7.50	26.93	2015.9	9853.2	1240.	8.42	36.66	0.230	0.890
134.0	56.0	7.50	27.58	2077.9	9865.9	1203.	8.37	35.61	0.235	0.896
135.0	55.6	7.50	27.76	2093.4	9869.1	1194.	8.36	35.36	0.236	0.898
140.0	53.6	7.50	28.68	2170.9	9885.6	1152.	8.30	34.15	0.243	0.904

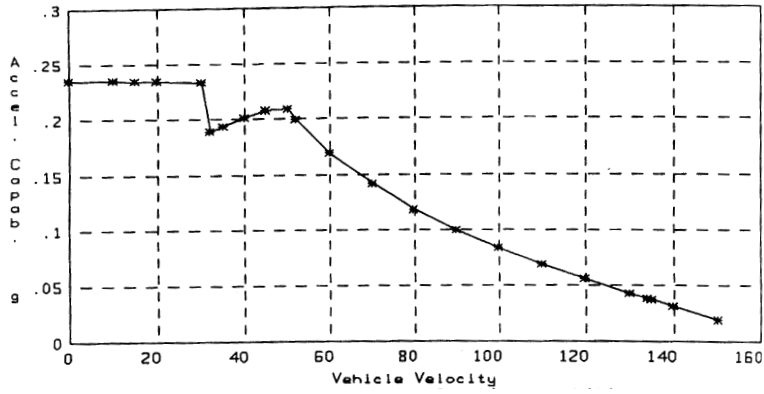
a. LSM thrust vs. speed, maximum thrust.



U_s (m/s)	F_x (kN)	F_t (kN)	V_s (V)	I_s (A)	P_s (MW)	S_s (MVA)	PF (PU)	E_{ff} (PU)
10.0	150.00	35.18	2425.7	3224.4	12.074	23.465	0.515	0.124
15.0	150.00	35.32	3389.9	3224.4	12.824	32.792	0.391	0.175
20.0	150.00	35.50	4390.3	3224.4	13.574	42.468	0.320	0.221
30.0	150.00	36.04	6431.6	3224.4	15.074	62.214	0.242	0.299
32.0	150.00	36.04	6843.1	3224.4	15.374	66.195	0.232	0.312
35.0	150.00	35.92	7461.5	3224.4	15.824	72.177	0.219	0.332
40.0	150.00	35.37	8494.5	3224.4	16.574	82.170	0.202	0.362
45.0	150.00	34.34	9529.7	3224.4	17.324	92.184	0.188	0.390
50.0	150.00	33.90	10566.4	3224.4	18.074	102.212	0.177	0.415
52.0	144.23	34.46	10564.5	3100.4	17.276	98.263	0.176	0.434
60.0	125.00	31.87	10561.7	2687.0	14.843	85.138	0.174	0.505
70.0	107.14	28.14	10566.1	2303.2	12.895	73.006	0.177	0.582
80.0	93.75	25.91	10576.4	2015.3	11.630	63.942	0.182	0.645
90.0	83.33	24.76	10591.0	1791.3	10.763	56.917	0.189	0.697
100.0	75.00	24.42	10609.3	1612.2	10.143	51.313	0.198	0.739
110.0	68.18	24.74	10630.6	1465.6	9.685	46.742	0.207	0.774
120.0	62.50	25.61	10654.8	1343.5	9.336	42.944	0.217	0.803
130.0	57.69	26.93	10681.5	1240.2	9.064	39.740	0.228	0.827
134.0	55.97	27.58	10692.9	1203.1	8.972	38.595	0.232	0.836
135.0	55.56	27.76	10695.8	1194.2	8.950	38.320	0.234	0.838
140.0	53.57	28.68	10710.7	1151.6	8.849	37.003	0.239	0.848

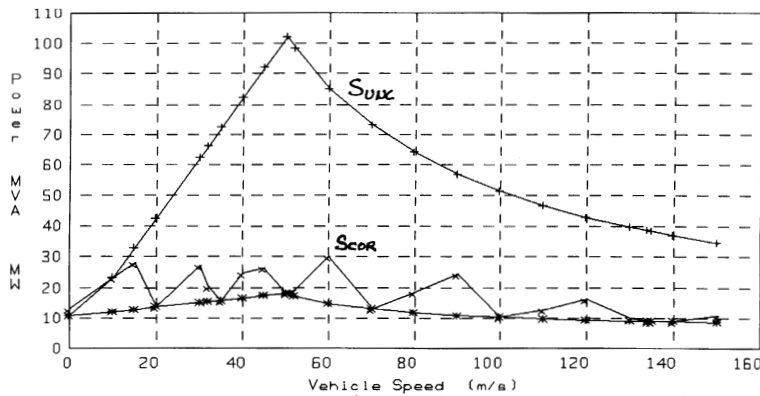
b. Converter station output power, maximum thrust.

Figure 41. Performance capability of the Magneplane SCD LSM.



U_s (m/s)	F_x (kN)	F_c (kN)	Accel (g)	Accel (m/s ²)
0.0	150.00	35.08	0.234	2.298
10.0	150.00	35.18	0.234	2.296
15.0	150.00	35.32	0.234	2.294
20.0	150.00	35.50	0.234	2.290
30.0	150.00	36.04	0.232	2.279
32.0	150.00	57.34	0.189	1.853
35.0	150.00	54.92	0.194	1.902
40.0	150.00	51.37	0.201	1.973
45.0	150.00	48.34	0.207	2.033
50.0	150.00	47.90	0.208	2.042
52.0	144.23	46.46	0.199	1.955
60.0	125.00	41.87	0.170	1.663
70.0	107.14	38.14	0.141	1.380
80.0	93.75	35.91	0.118	1.157
90.0	83.33	34.76	0.099	0.972
100.0	75.00	34.42	0.083	0.812
110.0	68.18	34.74	0.068	0.669
120.0	62.50	35.61	0.055	0.538
130.0	57.69	36.93	0.042	0.415
134.0	55.97	37.58	0.038	0.368
135.0	55.56	37.76	0.036	0.356
140.0	53.57	38.68	0.030	0.298

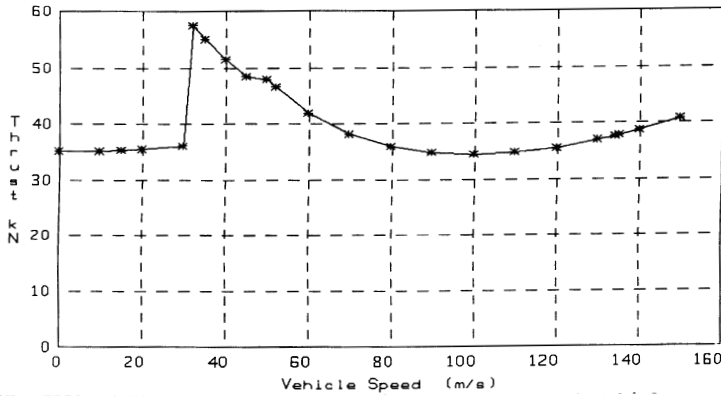
c. Acceleration capability, maximum thrust.



U_s (m/s)	F_x (kN)	F_c (kN)	V_s (V)	I_s (A)	P_s (MW)	S_s (MVA)	PF (PU)	E_{eff} (PU)	C_{pf} (uF)
0.0	150.00	35.08	1336.9	3224.4	10.574	12.932	0.818	0.000	1E12
10.0	150.00	35.18	2425.7	3224.4	12.074	23.465	0.515	0.124	1E12
15.0	150.00	35.32	2902.5	3224.4	12.824	28.076	0.457	0.175	9000
20.0	150.00	35.50	1408.0	3224.4	13.574	13.620	0.997	0.221	9000
30.0	150.00	36.04	2789.0	3224.4	15.074	26.979	0.559	0.299	3000
32.0	150.00	57.34	2093.4	3224.4	15.374	20.250	0.759	0.312	3000
35.0	150.00	54.92	1636.6	3224.4	15.824	15.831	1.000	0.332	3000
40.0	150.00	51.37	2562.3	3224.4	16.574	24.786	0.669	0.362	3000
45.0	150.00	48.34	2717.6	3224.4	17.324	26.289	0.659	0.390	1500
50.0	150.00	47.90	1873.4	3224.4	18.074	18.122	0.997	0.415	1500
52.0	144.23	46.46	2068.6	3100.4	17.276	19.240	0.898	0.434	1500
60.0	125.00	41.87	3754.9	2687.0	14.843	30.268	0.490	0.505	1500
70.0	107.14	38.14	1867.7	2303.2	12.895	12.905	0.999	0.582	750
80.0	93.75	35.91	3061.4	2015.3	11.630	18.508	0.628	0.645	750
90.0	83.33	34.76	4531.1	1791.3	10.763	24.350	0.442	0.697	750
100.0	75.00	34.42	2101.6	1612.2	10.143	10.165	0.998	0.739	375
110.0	68.18	34.74	2920.4	1465.6	9.685	12.841	0.754	0.774	375
120.0	62.50	35.61	4009.2	1343.5	9.336	16.159	0.578	0.803	375
130.0	57.69	36.93	2628.7	1240.2	9.064	9.780	0.927	0.827	200
134.0	55.97	37.58	2506.0	1203.1	8.972	9.045	0.992	0.836	200
135.0	55.56	37.76	2503.3	1194.2	8.950	8.969	0.998	0.838	200
140.0	53.57	38.68	2626.5	1151.6	8.849	9.074	0.975	0.848	200

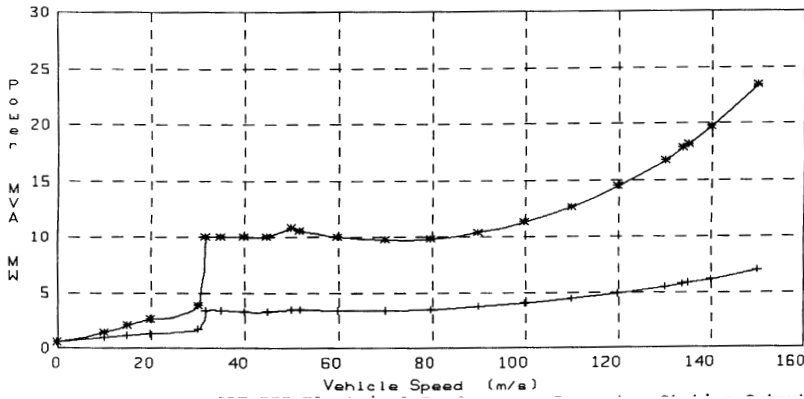
d. Converter station output power with power factor correction, maximum thrust.

Figure 41 (cont'd).



e. LSM thrust vs. speed, normal thrust.

U_s (m/s)	F_x (kN)	P_x (MW)	E_1 (V)	V_1 (V)	I_1 (A)	P (MW)	S (MVA)	PF (PU)	E_{ff} (PU)
0.0	35.08	0.00	0.0	150.8	754.0	0.34	0.34	1.000	0.000
10.0	35.18	0.35	155.1	544.2	756.3	0.70	1.23	0.563	0.506
15.0	35.32	0.53	232.6	778.8	759.2	0.88	1.77	0.494	0.605
20.0	35.50	0.71	310.1	1019.1	763.2	1.06	2.33	0.454	0.670
30.0	36.04	1.08	465.2	1515.2	774.7	1.44	3.52	0.409	0.750
32.0	57.34	1.83	496.2	2460.7	1232.5	2.75	9.10	0.302	0.668
35.0	54.92	1.92	542.7	2578.4	1180.6	2.76	9.13	0.302	0.697
40.0	51.37	2.05	620.3	2758.4	1104.2	2.79	9.14	0.305	0.737
45.0	48.34	2.18	697.8	2925.1	1039.1	2.82	9.12	0.310	0.771
50.0	47.90	2.40	775.3	3215.9	1029.8	3.03	9.93	0.305	0.790
52.0	46.46	2.42	806.3	3248.6	998.7	3.01	9.73	0.310	0.801
60.0	41.87	2.51	930.4	3399.0	900.1	3.00	9.18	0.327	0.838
70.0	38.14	2.67	1085.5	3634.8	819.8	3.07	8.94	0.344	0.869
80.0	35.91	2.87	1240.5	3929.1	771.9	3.23	9.10	0.355	0.889
90.0	34.76	3.13	1395.6	4287.8	747.2	3.46	9.61	0.360	0.903
100.0	34.42	3.44	1550.7	4717.9	740.0	3.77	10.47	0.360	0.913
110.0	34.74	3.82	1705.7	5226.8	746.8	4.16	11.71	0.355	0.919
120.0	35.61	4.27	1860.8	5822.4	765.4	4.62	13.37	0.346	0.924
130.0	36.93	4.80	2015.9	6512.9	793.9	5.18	15.51	0.334	0.927
134.0	37.58	5.04	2077.9	6817.6	807.9	5.43	16.52	0.328	0.928
135.0	37.76	5.10	2093.4	6896.5	811.6	5.49	16.79	0.327	0.928
140.0	38.68	5.41	2170.9	7307.0	831.4	5.83	18.22	0.320	0.929



f. Converter station output power, normal thrust.

U_s (m/s)	F_x (kN)	V_s (V)	I_s (A)	P_s (MW)	S_s (MVA)	PF (PU)	E_{ff} (PU)
0.0	35.08	255.6	754.0	0.578	0.578	1.000	0.000
10.0	35.18	638.2	756.3	0.934	1.448	0.645	0.377
15.0	35.32	883.0	759.2	1.116	2.011	0.555	0.475
20.0	35.50	1137.2	763.2	1.302	2.604	0.500	0.545
30.0	36.04	1666.6	774.7	1.692	3.874	0.437	0.639
32.0	57.34	2703.4	1232.5	3.380	9.996	0.338	0.543
35.0	54.92	2827.5	1180.6	3.340	10.015	0.334	0.576
40.0	51.37	3017.7	1104.2	3.295	9.996	0.330	0.624
45.0	48.34	3194.0	1039.1	3.273	9.957	0.329	0.665
50.0	47.90	3506.5	1029.8	3.474	10.833	0.321	0.690
52.0	46.46	3540.1	998.7	3.430	10.606	0.323	0.704
60.0	41.87	3696.6	900.1	3.337	9.982	0.334	0.753
70.0	38.14	3944.9	819.8	3.353	9.702	0.346	0.796
80.0	35.91	4257.4	771.9	3.479	9.859	0.353	0.826
90.0	34.76	4640.6	747.2	3.696	10.402	0.355	0.846
100.0	34.42	5102.1	740.0	3.999	11.327	0.353	0.861
110.0	34.74	5649.9	746.8	4.389	12.659	0.347	0.871
120.0	35.61	6292.6	765.4	4.868	14.449	0.337	0.878
130.0	36.93	7039.1	793.9	5.442	16.766	0.325	0.882
134.0	37.58	7368.9	807.9	5.700	17.860	0.319	0.884
135.0	37.76	7454.2	811.6	5.767	18.150	0.318	0.884
140.0	38.68	7898.7	831.4	6.118	19.700	0.311	0.885

Figure 41 (contd). Performance capability of the Magneplane SCD LSM.

resulting from power-factor correction. Through the speed range below 60 m/s, this correction reduces megavolt-ampere requirements by nearly a factor of 3; above 60 m/s, the reduction is about a factor of 2. The maximum megavolt-amperes for an uncorrected power factor was in excess of 100 at 50 m/s. The partial power-factor correction applied here reduced this maximum to 30 MVA at the same speed.

The efficiency of the LSM varies considerably over the vehicle's speed and is a direct result of the high LSM stator current required to meet the high thrust being produced. The efficiency peaks at 92% at the design point speed of 150 m/s.

The acceleration capability of the Magneplane LSM with a 50,000-kg vehicle exceeds 0.16 g for speeds up to 65 m/s. The maximum acceleration then falls rapidly with speed to 0.08 g at 100 m/s and 0.038 g at 134 m/s.

The uncorrected power factor is quite low across all speeds, being approximately 26% lagging at the design point speed. Power factor correction is expected to significantly improve the situation, and its effects on both efficiency and power factor can be considered by the LSMPOWER model once the implementation details are specified.

The LSM parameters used by LSMPOWER for the Magneplane concept closely match the corresponding parameters reported by Magneplane. The LSMPOWER performance results agree quite closely with those reported by Magneplane. A preliminary analysis of power-factor correction tells us that a significant improvement in the power factor is possible; this should result in significant energy savings. The incremental capital cost to make such a correction must be weighed against the potential energy cost savings.

Bechtel. The Bechtel LSM is an air-core machine with conventional stator windings mounted on the box beam sidewalls. There are two LSMs per vehicle, each with a sidewall air gap of approximately 0.10 m. Superconducting propulsion coils are located on distributed bogies along each side of the vehicle. The stator coils are configured as a six-phase system, with one set of stator windings located on the upper portion of the box-beam sidewall and a second set on the lower portion. The baseline vehicle is a one-car consist.

The LSM blocklengths are 2000 m for the baseline concept and are end-fed from the converter stations. Converter stations are located at every other blocklength and are assumed to be located under the guideway so as to not require feeder

cables of any significant length. High-voltage DC (30,000-V) is obtained from rectifier stations located at each utility interface and this voltage is transmitted along the guideway to the frequency converter stations.

We produced the following performance data using the LSMPOWER model for the Bechtel LSM concept operating as described above.

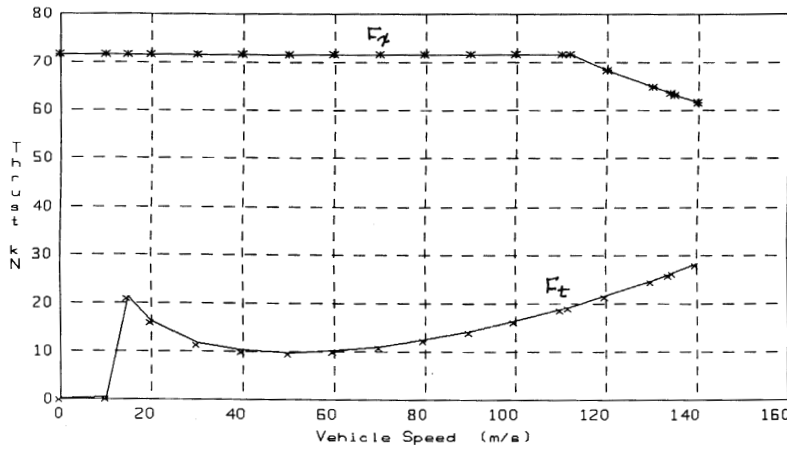
Blocklength resistance R_L :	0.16 Ω
Blocklength inductance L_L :	0.0016 H
Vehicle magnetic length l_v :	2000 m
Longitudinal length of stator L :	2000 m
Field winding pole pitch t_p :	1.0 m
Width of LSM stator l :	0.30 m
Pole pairs per LSM p :	12
Slots per pole per phase N :	2
Number of phases N_p :	6
Number of LSMs per consist N_m :	2
Resistance of feeder cable R_f :	0 Ω
Inductance of feeder cable L_f :	0 H
Air gap flux density:	0.90 T
Maximum stator current per LSM:	1300 A
Maximum power per LSM:	11 MVA

The above data were obtained from information provided by Bechtel and MIT at the IPR and from the SCD final report; where possible, they were independently verified through calculation. The above data show the magnetic length of the vehicle to be equal to the LSM blocklength to account for circuit parameters specified by MIT.

Figure 42 summarizes the performance capability of the Bechtel LSM. The maximum thrust capability for a one-car consist is 143 kN. This concept provides constant thrust from 0 to 112 m/s and then operates at a constant power of 22 MVA for higher speeds. The acceleration capability for a 63,300-kg vehicle exceeds 0.16 g for speeds up to 118 m/s, and it exceeds 0.11 g at 135 m/s.

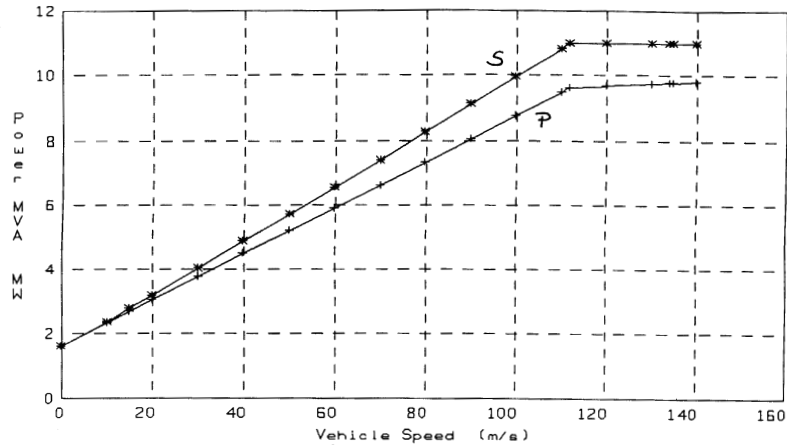
The efficiency of the LSM at maximum thrust varies considerably with speed and reaches 87% at 135 m/s. Under normal thrust conditions, the efficiency is relatively constant at about 90–92% for speeds above 50 m/s. The power factor is about 90% for maximum thrust conditions at most speeds and about 95% or more at nearly all speeds for nominal thrust conditions.

LSMPOWER predicted approximately the same results as those reported by Bechtel. Bechtel's plan to use power-factor correction resulted in the low inductance values input to LSMPOWER and apparently their own model. However, they didn't describe the specifics of this correction, and its relative improvements vs. its costs would need to be examined.



U_s (m/s)	F_x (kN)	F_t (kN)	E_1 (V)	V_1 (V)	I_1 (A)	P (MW)	S (MVA)	PF (PU)
0.0	71.5	0.3	0.0	208.0	1300	1.62	1.62	1.000
10.0	71.5	0.4	91.6	305.8	1300	2.34	2.39	0.980
15.0	71.5	21.4	137.5	357.5	1300	2.69	2.79	0.966
20.0	71.5	16.3	183.3	410.0	1300	3.05	3.20	0.954
30.0	71.5	11.8	274.9	516.7	1300	3.77	4.03	0.935
40.0	71.5	10.1	366.6	624.6	1300	4.48	4.87	0.920
50.0	71.5	9.7	458.2	733.2	1300	5.20	5.72	0.909
60.0	71.5	10.1	549.8	842.3	1300	5.91	6.57	0.900
70.0	71.5	11.1	641.5	951.6	1300	6.63	7.42	0.893
80.0	71.5	12.5	733.1	1061.1	1300	7.34	8.28	0.887
90.0	71.5	14.3	824.8	1170.7	1300	8.06	9.13	0.882
100.0	71.5	16.5	916.4	1280.5	1300	8.77	9.99	0.878
110.0	71.5	18.9	1008.1	1390.3	1300	9.49	10.84	0.875
111.8	71.5	19.4	1024.7	1410.2	1300	9.62	11.00	0.874
120.0	68.3	21.7	1099.7	1476.2	1242	9.68	11.00	0.880
130.0	64.7	24.8	1191.3	1556.9	1178	9.75	11.00	0.886
134.0	63.4	26.1	1228.0	1589.3	1154	9.78	11.00	0.889
135.0	63.1	26.4	1237.2	1597.4	1148	9.78	11.00	0.889
140.0	61.5	28.1	1283.0	1638.0	1119	9.82	11.00	0.893

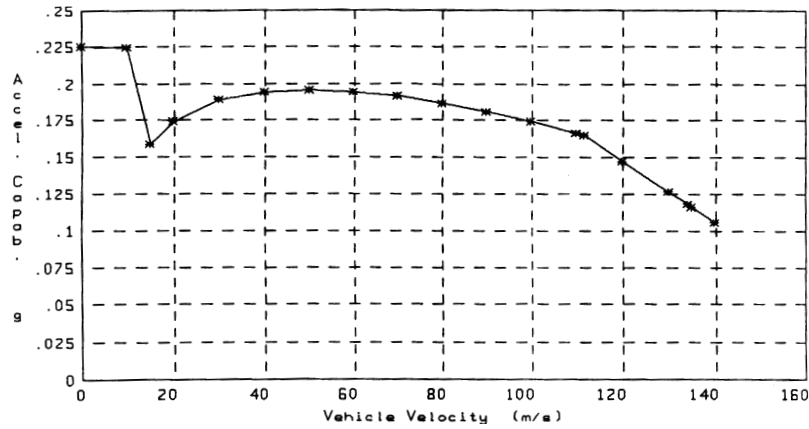
a. LSM thrust vs. speed, maximum thrust.



U_s (m/s)	F_x (kN)	F_t (kN)	V_s (V)	I_s (A)	P_s (MW)	S_s (MVA)	PF (PU)	E_{eff} (PU)
0.0	71.5	0.3	208	1300	1.622	1.622	1.000	0.000
10.0	71.5	0.4	306	1300	2.337	2.386	0.980	0.306
15.0	71.5	21.4	357	1300	2.695	2.788	0.966	0.398
20.0	71.5	16.3	410	1300	3.052	3.198	0.954	0.468
30.0	71.5	11.8	517	1300	3.767	4.030	0.935	0.569
40.0	71.5	10.1	625	1300	4.482	4.872	0.920	0.638
50.0	71.5	9.7	733	1300	5.196	5.719	0.909	0.688
60.0	71.5	10.1	842	1300	5.911	6.570	0.900	0.726
70.0	71.5	11.1	952	1300	6.626	7.422	0.893	0.755
80.0	71.5	12.5	1061	1300	7.341	8.276	0.887	0.779
90.0	71.5	14.3	1171	1300	8.056	9.132	0.882	0.799
100.0	71.5	16.5	1280	1300	8.770	9.988	0.878	0.815
110.0	71.5	18.9	1390	1300	9.485	10.844	0.875	0.829
111.8	71.5	19.4	1410	1300	9.615	11.000	0.874	0.831
120.0	68.3	21.7	1476	1242	9.675	11.000	0.880	0.847
130.0	64.7	24.8	1557	1178	9.748	11.000	0.886	0.863
134.0	63.4	26.1	1589	1154	9.777	11.000	0.889	0.869
135.0	63.1	26.4	1597	1148	9.784	11.000	0.889	0.871
140.0	61.5	28.1	1638	1119	9.819	11.000	0.893	0.878

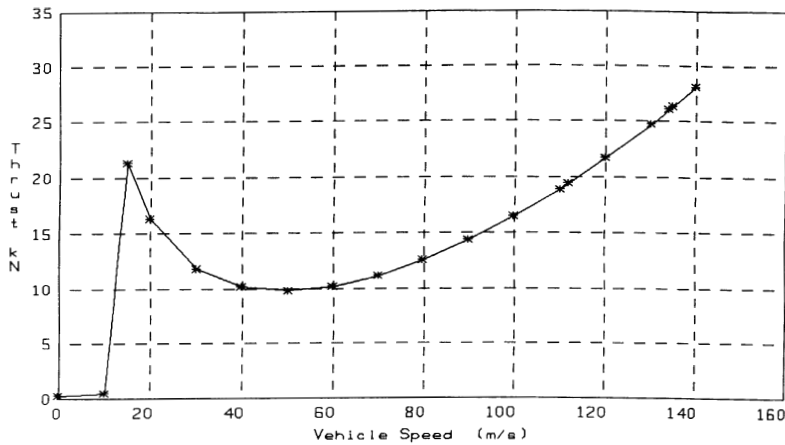
b. Converter station output power, maximum thrust.

Figure 42. Performance capability of Bechtel SCD LSM.



U _s (m/s)	F _x (kN)	F _z (kN)	Accel (g)	Accel (m/s ²)
0.0	71.5	0.3	0.225	2.207
10.0	71.5	0.4	0.225	2.203
15.0	71.5	21.4	0.159	1.554
20.0	71.5	16.3	0.174	1.709
30.0	71.5	11.8	0.189	1.851
40.0	71.5	10.1	0.194	1.903
50.0	71.5	9.7	0.195	1.915
60.0	71.5	10.1	0.194	1.902
70.0	71.5	11.1	0.191	1.872
80.0	71.5	12.5	0.186	1.828
90.0	71.5	14.3	0.181	1.772
100.0	71.5	16.5	0.174	1.706
110.0	71.5	18.9	0.166	1.630
111.8	71.5	19.4	0.165	1.615
120.0	68.3	21.7	0.147	1.445
130.0	64.7	24.8	0.126	1.240
134.0	63.4	26.1	0.118	1.159
135.0	63.1	26.4	0.116	1.138
140.0	61.5	28.1	0.106	1.037

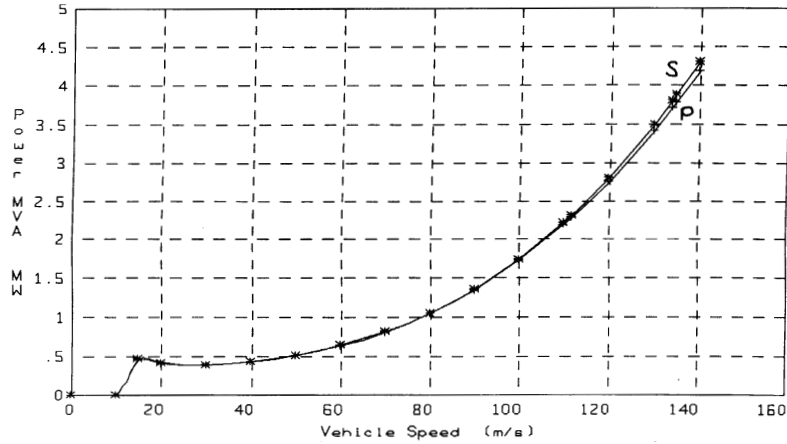
c. Acceleration capability, maximum thrust.



U _s (m/s)	F _x (kN)	E ₁ (V)	V ₁ (V)	I ₁ (A)	P (MW)	S (MVA)	PF (PU)
0.0	0.32	0.0	0.9	6	0.000	0.000	1.000
10.0	0.45	91.6	92.9	8	0.005	0.005	1.000
15.0	21.35	137.5	201.5	388	0.465	0.469	0.991
20.0	16.35	183.3	232.6	297	0.412	0.415	0.993
30.0	11.79	274.9	310.7	214	0.398	0.400	0.995
40.0	10.10	366.6	397.5	184	0.437	0.438	0.996
50.0	9.73	458.2	488.3	177	0.517	0.519	0.996
60.0	10.14	549.8	581.7	184	0.641	0.644	0.996
70.0	11.11	641.5	677.1	202	0.817	0.821	0.995
80.0	12.52	733.1	774.3	228	1.052	1.058	0.994
90.0	14.32	824.8	873.4	260	1.354	1.365	0.992
100.0	16.46	916.4	974.6	299	1.732	1.750	0.989
110.0	18.92	1008.1	1078.0	344	2.195	2.226	0.986
111.8	19.40	1024.7	1097.0	353	2.289	2.323	0.986
120.0	21.69	1099.7	1184.0	394	2.752	2.803	0.982
130.0	24.75	1191.3	1293.1	450	3.413	3.493	0.977
134.0	26.06	1228.0	1337.7	474	3.708	3.804	0.975
135.0	26.39	1237.2	1349.0	480	3.784	3.885	0.974
140.0	28.10	1283.0	1405.8	511	4.185	4.311	0.971

d. LSM thrust vs. speed, normal thrust.

Figure 42 (cont'd)



U_s (m/s)	F_t (kN)	V_s (V)	I_s (A)	P_s (MW)	S_s (MVA)	PF (PU)	E_{eff} (PU)
0.0	0.32	1	6	0.000	0.000	1.000	0.000
10.0	0.45	93	8	0.005	0.005	1.000	0.986
15.0	21.35	201	388	0.465	0.469	0.991	0.689
20.0	16.35	233	297	0.412	0.415	0.993	0.794
30.0	11.79	311	214	0.398	0.400	0.995	0.889
40.0	10.10	397	184	0.437	0.438	0.996	0.926
50.0	9.73	488	177	0.517	0.519	0.996	0.942
60.0	10.14	582	184	0.641	0.644	0.996	0.949
70.0	11.11	677	202	0.817	0.821	0.995	0.952
80.0	12.52	774	228	1.052	1.058	0.994	0.953
90.0	14.32	873	260	1.354	1.365	0.992	0.952
100.0	16.46	975	299	1.732	1.750	0.989	0.950
110.0	18.92	1078	344	2.195	2.226	0.986	0.948
111.8	19.40	1097	353	2.289	2.323	0.986	0.948
120.0	21.69	1184	394	2.752	2.803	0.982	0.946
130.0	24.75	1293	450	3.413	3.493	0.977	0.943
134.0	26.06	1338	474	3.708	3.804	0.975	0.942
135.0	26.39	1349	480	3.784	3.885	0.974	0.942
140.0	28.10	1406	511	4.185	4.311	0.971	0.940

e. Converter station output power, normal thrust.

Figure 42 (cont'd). Performance capability of Bechtel SCD LSM.

Foster-Miller. The Foster-Miller LSM is an air-core machine where the LSM coils are located on both channel-guideway sidewalls. The sidewall air gap is approximately 100 mm. Superconducting propulsion coils are located on bogies at each end of the vehicle and with a shared bogie for each car section. The pole pitch of the propulsion coils mounted on the vehicle is different from the coils mounted on the sidewall, the ratio being approximately 1.5:1 vehicle coil to guideway coil.

The propulsion coils are individually controlled by adjacent solid-state bridges (H-bridges) installed in the guideway, and the concept is called a Locally Commutated Linear Synchronous Motor (LCLSM). These LSM coils do not overlap and three-phase operation is obtained electronically by control of the H-bridges. The sequence of control of the propulsion coils is to energize a set of LSM coils at the instant a bogie is opposite them. The idea is to synthesize a traveling wave down the guideway to propel the vehicle, but only those coils adjacent to vehicle magnets are energized at any time.

High-voltage DC (2100 V) is obtained from rectifier stations located at approximately every 8000 m. This DC power is distributed along the guideway to each of the LCLSMs. Each of the opposite LSM coils in the guideway sidewalls is connected electrically in parallel to the H-bridge. For the baseline two-car consist, this is equivalent to 18 individual LSMs powering it. For an eight-car consist, this is equivalent to 54 individual LSMs.

A key function of the LCLSM control system is to alternately switch the propulsion coils from a thrust mode to a power transfer mode as the vehicle moves down the guideway. The LCLSM coils that are located between the bogies are operated as an air-core transformer interacting with a vehicle-mounted coil to transfer power from the guideway to the vehicle.

We produced performance data using the LSMPOWER model for the Foster-Miller LSM concept operating as described above.

Blocklength resistance R_L :	0.0049 Ω
Blocklength inductance L_L :	0.000123 H
Vehicle magnetic length L_v :	4000 m

Longitudinal length of stator L :	4000 m
Field winding pole pitch t_p :	1.3 m
Width of LSM stator l :	0.7 m
Pole pairs per LSM p :	1
Number of conductors per winding:	11
Number of phases N_p :	1
Number of LSMs per consist N_m :	18
Resistance of feeder cable R_f :	0.38 Ω
Inductance of feeder cable L_f :	0 H
Back EMF characteristics at a specified speed E_1 :	1370 V at 135 m/s
Maximum stator current per LSM pair:	857 A
Maximum power per LSM pair:	0.74 MW

The above data were obtained from information provided by Foster-Miller during the IPRs, from the SCD final report, and from supplemental material provided by Foster-Miller. Where possible the data were independently verified through calculation.

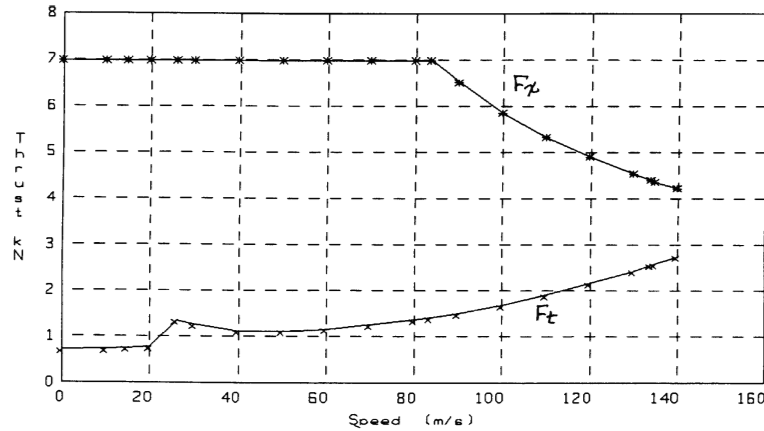
Figure 43 summarizes the performance capability of the Foster-Miller SCD LSM. The maximum thrust capability of the LCLSM for the two-car consist was 7 kN per LSM, or a total of 126 kN for the consist. The thrust-speed breakpoint from con-

stant thrust to constant power occurs at 83.5 m/s, where the consist power limit is set to 10.6 MW. Similar performance exists for an eight-car consist, with the maximum power scaling to 31.9 MW.

The acceleration capability for a two-car consist of 72,700 kg exceeds 0.14 g for speeds up to 83.5 m/s. Above this speed, acceleration capability decreases nearly linearly to 0.05 g at 135 m/s. The eight-car consist shows similar performance, except that the maximum acceleration is about 0.13 g. This results from a slight reduction in the allowable maximum current for each LSM.

The efficiency of the LCLSM is essentially constant over a wide speed range. It exceeds 99% at the output of the H-bridge and is approximately 95% at the output of the rectifier station. The power factor at the output of the H-bridge is approximately 80% lagging and is essentially constant over the entire speed range.

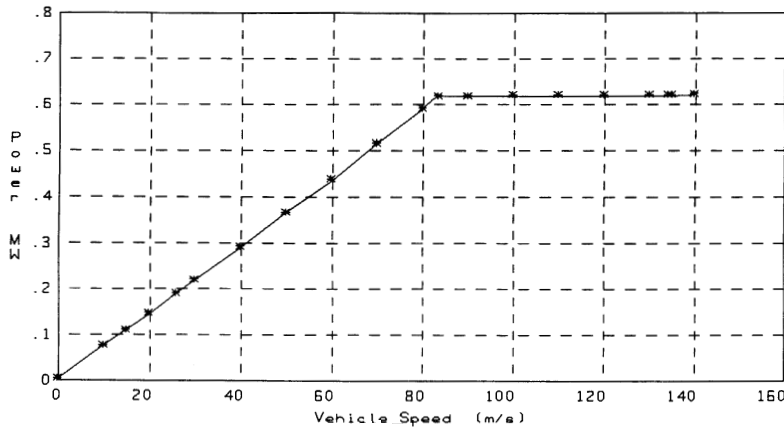
The current requirement for the H-bridge devices is approximately 860 A per device for maximum thrust. The high switching speeds intended for the H-bridge devices will probably require them to be



U_s (m/s)	F_x (kN)	F_c (kN)	E_1 (V)	V_1 (V)	I_1 (A)	P (MW)	S (MVA)	PF (PU)	E_{eff} (PU)
0.0	6.99	0.71	0.1	4.2	857.0	0.004	0.004	1.000	0.010
10.0	6.99	0.73	101.5	106.4	857.0	0.074	0.091	0.806	0.951
15.0	6.99	0.74	152.2	157.9	857.0	0.108	0.135	0.802	0.967
20.0	6.99	0.76	203.0	209.4	857.0	0.143	0.179	0.799	0.975
26.0	6.99	1.33	263.9	271.2	857.0	0.185	0.232	0.798	0.981
30.0	6.99	1.24	304.4	312.4	857.0	0.213	0.268	0.797	0.983
40.0	6.99	1.12	405.9	415.4	857.0	0.283	0.356	0.796	0.987
50.0	6.99	1.11	507.4	518.4	857.0	0.353	0.444	0.795	0.990
60.0	6.99	1.16	608.9	621.4	857.0	0.423	0.533	0.794	0.991
70.0	6.99	1.25	710.4	724.4	857.0	0.493	0.621	0.794	0.993
80.0	6.99	1.35	811.9	827.5	857.0	0.563	0.709	0.794	0.994
83.5	6.99	1.40	847.3	863.5	857.0	0.587	0.740	0.794	0.994
90.0	6.50	1.50	913.3	929.3	796.3	0.588	0.740	0.794	0.995
100.0	5.86	1.68	1014.8	1030.5	718.1	0.588	0.740	0.795	0.996
110.0	5.33	1.90	1116.3	1131.7	653.9	0.589	0.740	0.796	0.996
120.0	4.90	2.15	1217.8	1233.0	600.2	0.589	0.740	0.796	0.997
130.0	4.52	2.43	1319.3	1334.3	554.6	0.590	0.740	0.797	0.997
134.0	4.39	2.55	1359.9	1374.8	538.3	0.590	0.740	0.797	0.998
135.0	4.36	2.58	1370.0	1384.9	534.3	0.590	0.740	0.797	0.998

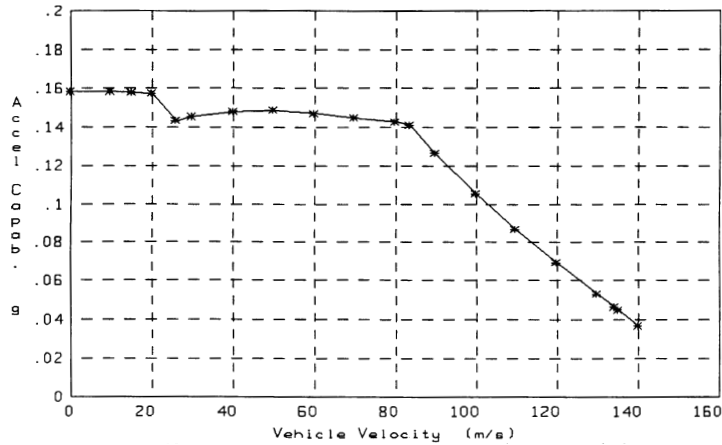
a. LSM thrust vs. speed, maximum thrust.

Figure 43. Performance capability of Foster-Miller SCD LSM.



b. Converter station output power, maximum thrust.

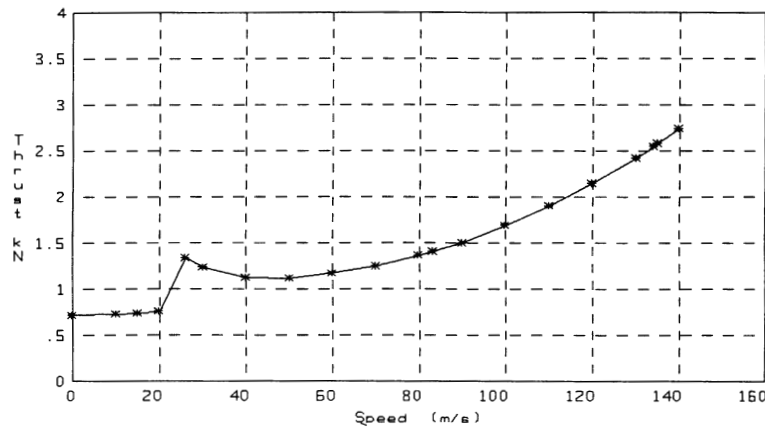
U_s (m/s)	F_x (kN)	F_t (kN)	V_s (V)	V_L (V)	$V_s L$ (V)	I_L (A)	P_s (MW)	E_{eff} (PU)
0.0	6.99	0.71	2101.0	2100.0	1.02	2.7	0.006	0.006
10.0	6.99	0.73	2113.7	2100.0	13.66	36.0	0.076	0.920
15.0	6.99	0.74	2120.0	2100.0	19.99	52.6	0.112	0.940
20.0	6.99	0.76	2126.3	2100.0	26.31	69.2	0.147	0.950
26.0	6.99	1.33	2133.9	2100.0	33.90	89.2	0.190	0.955
30.0	6.99	1.24	2139.0	2100.0	38.96	102.5	0.219	0.956
40.0	6.99	1.12	2151.6	2100.0	51.62	135.8	0.292	0.957
50.0	6.99	1.11	2164.3	2100.0	64.27	169.1	0.366	0.955
60.0	6.99	1.16	2176.9	2100.0	76.92	202.4	0.441	0.952
70.0	6.99	1.25	2189.6	2100.0	89.57	235.7	0.516	0.948
80.0	6.99	1.35	2202.2	2100.0	102.22	269.0	0.592	0.944
83.5	6.99	1.40	2206.6	2100.0	106.64	280.6	0.619	0.943
90.0	6.50	1.50	2206.7	2100.0	106.72	280.8	0.620	0.943
100.0	5.86	1.68	2206.8	2100.0	106.83	281.1	0.620	0.944
110.0	5.33	1.90	2206.9	2100.0	106.92	281.4	0.621	0.945
120.0	4.90	2.15	2207.0	2100.0	107.00	281.6	0.621	0.945
130.0	4.52	2.43	2207.1	2100.0	107.06	281.7	0.622	0.946
134.0	4.39	2.55	2207.1	2100.0	107.09	281.8	0.622	0.946
135.0	4.36	2.58	2207.1	2100.0	107.09	281.8	0.622	0.946



c. Acceleration capability, maximum thrust.

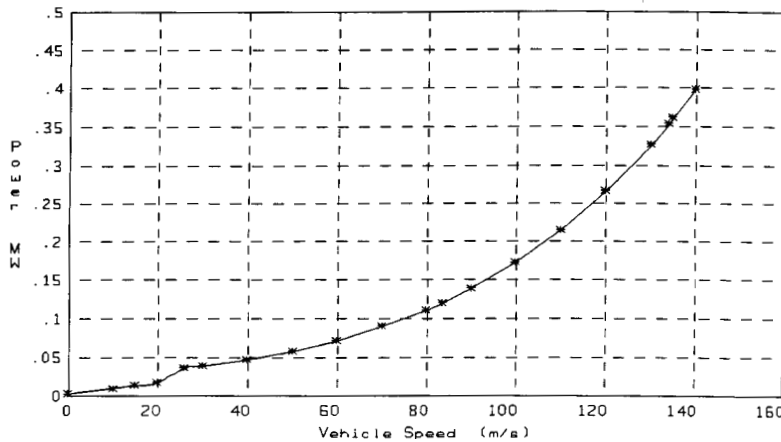
U_s (m/s)	F_x (kN)	F_t (kN)	Accel (g)	Accel (m/s ²)
0.0	6.99	0.71	0.158	1.554
10.0	6.99	0.73	0.158	1.551
15.0	6.99	0.74	0.158	1.547
20.0	6.99	0.76	0.157	1.542
26.0	6.99	1.33	0.143	1.401
30.0	6.99	1.24	0.145	1.425
40.0	6.99	1.12	0.148	1.454
50.0	6.99	1.11	0.148	1.456
60.0	6.99	1.16	0.147	1.443
70.0	6.99	1.25	0.145	1.421
80.0	6.99	1.35	0.142	1.395
83.5	6.99	1.40	0.141	1.384
90.0	6.50	1.50	0.126	1.237
100.0	5.86	1.68	0.105	1.033
110.0	5.33	1.90	0.087	0.850
120.0	4.90	2.15	0.069	0.679
130.0	4.52	2.43	0.053	0.518
134.0	4.39	2.55	0.046	0.456
135.0	4.36	2.58	0.045	0.440

Figure 43 (cont'd). Performance capability of Foster-Miller SCD LSM.



U_s (m/s)	F_t (kN)	E_1 (V)	V_1 (V)	I_1 (A)	P (MW)	S (MVA)	FF (PU)	E_{eff} (PU)
0.0	0.71	0.1	0.5	87.4	0.000	0.000	0.998	0.087
10.0	0.73	101.5	102.0	88.9	0.007	0.009	0.804	0.995
15.0	0.74	152.2	152.8	90.8	0.011	0.014	0.804	0.996
20.0	0.76	203.0	203.7	93.4	0.015	0.019	0.803	0.997
26.0	1.23	263.9	265.2	163.3	0.035	0.043	0.803	0.996
30.0	1.24	304.4	305.8	151.4	0.037	0.046	0.803	0.997
40.0	1.12	405.9	407.4	137.2	0.045	0.056	0.803	0.998
50.0	1.11	507.4	509.1	136.0	0.056	0.069	0.802	0.998
60.0	1.16	608.9	611.0	142.7	0.070	0.087	0.802	0.999
70.0	1.25	710.4	712.9	153.4	0.088	0.109	0.802	0.999
80.0	1.35	811.9	814.9	166.1	0.109	0.135	0.802	0.999
83.5	1.40	847.4	850.6	171.8	0.117	0.146	0.802	0.999
90.0	1.50	913.3	917.0	184.0	0.135	0.169	0.802	0.999
100.0	1.68	1014.8	1019.3	206.5	0.169	0.211	0.801	0.999
110.0	1.90	1116.3	1121.8	233.2	0.210	0.262	0.801	0.999
120.0	2.15	1217.8	1224.4	263.7	0.258	0.323	0.801	0.999
130.0	2.43	1319.3	1327.3	297.9	0.316	0.395	0.800	0.999
134.0	2.55	1359.9	1368.5	312.5	0.342	0.428	0.800	0.999
135.0	2.58	1370.0	1378.8	316.3	0.349	0.436	0.800	0.999

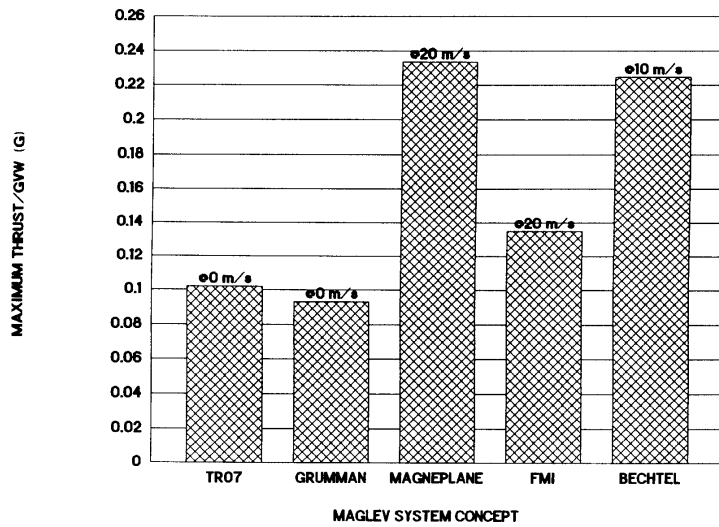
d. LSM thrust vs. speed, normal thrust.



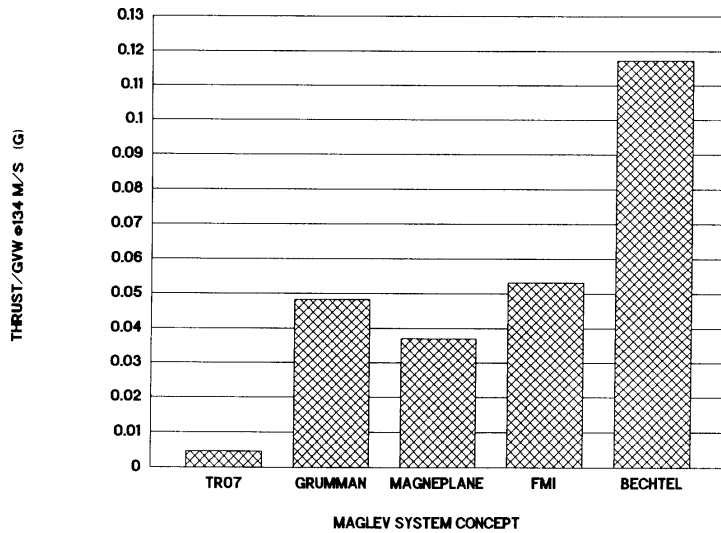
U_s (m/s)	F_t (kN)	V_s (V)	VL (V)	$V_s I_s$ (V)	IL (A)	P_s (MW)	E_{eff} (PU)
0.0	0.71	2100.4	2100.0	0.37	1.0	0.002	0.002
10.0	0.73	2101.7	2100.0	1.68	4.4	0.009	0.780
15.0	0.74	2102.4	2100.0	2.38	6.3	0.013	0.844
20.0	0.76	2103.1	2100.0	3.13	8.2	0.017	0.880
26.0	1.33	2106.7	2100.0	6.65	17.5	0.037	0.939
30.0	1.24	2107.1	2100.0	7.09	18.7	0.039	0.943
40.0	1.12	2108.5	2100.0	8.48	22.3	0.047	0.952
50.0	1.11	2110.4	2100.0	10.41	27.4	0.058	0.959
60.0	1.16	2113.0	2100.0	13.02	34.3	0.072	0.965
70.0	1.25	2116.2	2100.0	16.23	42.7	0.090	0.969
80.0	1.35	2120.0	2100.0	20.00	52.6	0.112	0.971
83.5	1.40	2121.6	2100.0	21.57	56.8	0.120	0.972
90.0	1.50	2124.8	2100.0	24.84	65.4	0.139	0.973
100.0	1.68	2130.9	2100.0	30.89	81.3	0.173	0.973
110.0	1.90	2138.3	2100.0	38.28	100.7	0.215	0.972
120.0	2.15	2147.1	2100.0	47.14	124.0	0.266	0.969
130.0	2.43	2157.6	2100.0	57.60	151.6	0.327	0.966
134.0	2.55	2162.3	2100.0	62.27	163.9	0.354	0.964
135.0	2.58	2163.5	2100.0	63.48	167.1	0.361	0.964

e. Converter station output power, normal thrust.

Figure 43 (cont'd).



a. Low speed.



b. 134 m/s.

Figure 44. Comparison of acceleration capabilities.

IGBTs (insulated gate bipolar transistors), since the switching speeds required are beyond those recommended for GTOs (gate turnoff thyristors). Current commercially available IGBTs are limited to 600-A ratings with voltage ratings of 1400 V, such as the soon to be introduced Fuji device. Using devices of this type in the LCLSM would require at least two in series and two in parallel per H-bridge leg, or a total of at least 12 devices per H-bridge. The continuing evolution of IGBTs will probably reduce this to six devices per H-bridge within the foreseeable future.

The performance results from LSMPOWER compare well to those reported by Foster-Miller. However, the controllability of the LCLSM is an important technical issue that was not addressed in this analysis. It would require additional effort that would perhaps be best handled with an experi-

mental scale model of the LCLSM. Section 4.4 and Appendix C of this report give more detail about the risks and benefits of this innovative propulsion concept.

Comparative performance of the LSM concepts

The results of the LSMPOWER runs for each of the SCD concepts and the TR07 were compared for their relative performance in acceleration and grade climbing capability. The SCD RFP (USDOTFRA 1991) required that the system concepts be able to maintain the maximum cruising speed on a +3.5% grade, and that, further, they be capable of operating at some speed on a +10% grade.

Acceleration capability. Figure 44a gives the low-speed acceleration capability for the five systems

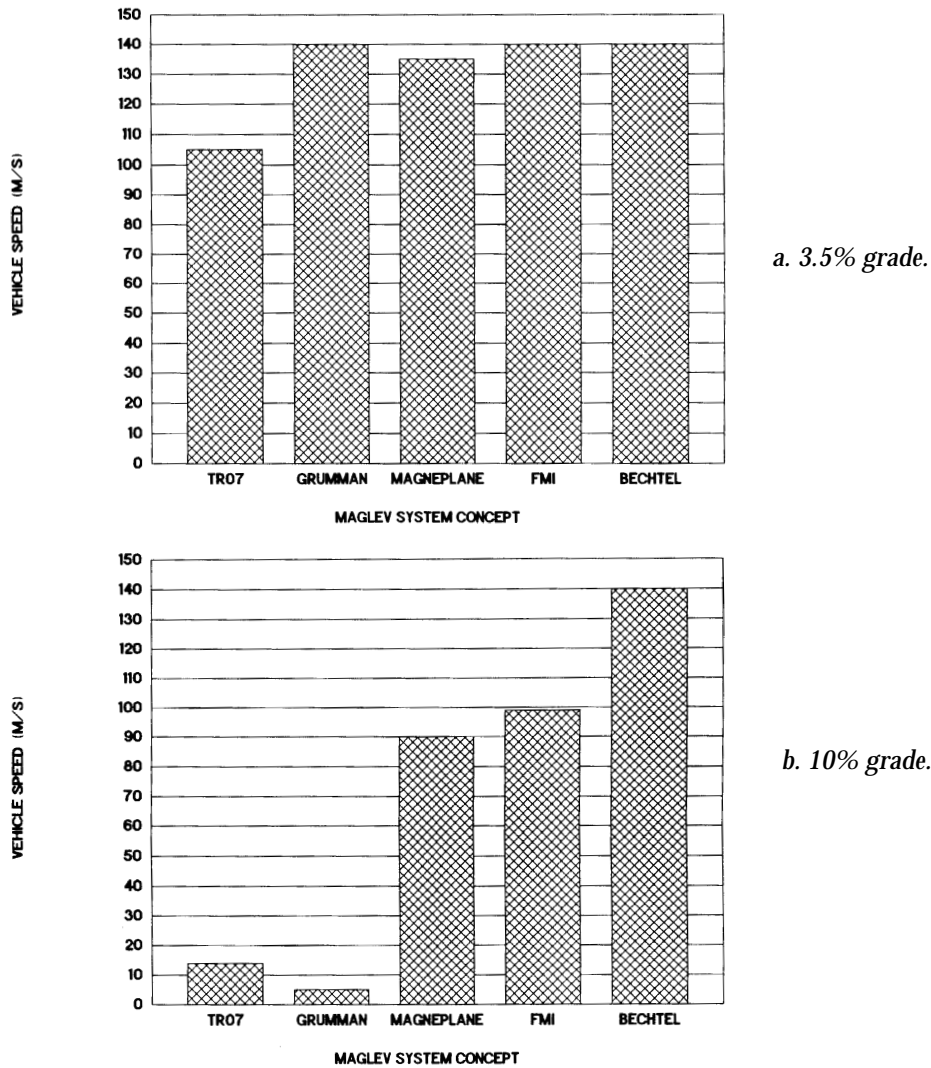


Figure 45. Comparison of speeds sustained on grades.

analyzed. The maximum acceleration capabilities at the zero liftoff speed for the TR07 and Grumman baseline SCD are 0.102 and 0.093 g, respectively. Grumman's optional 100-kN LSM increases its maximum acceleration to 0.16 g. For the EDS concepts, the acceleration capabilities at a 20-m/s liftoff speed for the Magneplane and Foster-Miller vehicles are 0.234 and 0.157 g, respectively. The Bechtel concept can achieve 0.226 g at its liftoff speed of 10 m/s.

Figure 44b shows that the acceleration capability remaining at the maximum cruise speed of 134 m/s is 0.006 g for TR07, 0.05 g for Grumman, 0.04 g for Magneplane, 0.05 g for Foster-Miller, and 0.12 g for Bechtel. Grumman's optional 100-kN LSM raises its value to 0.10 g.

Grade climbing capability. Figure 45a shows the maximum speeds that the SCDs and TR07 may

maintain up a 3.5% grade. These are the steady-state balance speeds and do not consider grade length and inertia to pass over the grade at some changing speed. Also, these calculations were based on the baseline configurations discussed earlier and do not account for any LSM configuration changes at the grade condition. Note that all SCD concepts are able to maintain maximum cruise speed up a 3.5% grade, as required. The 7.2-MVA power limit for the TR07 limits its 3.5%-grade-climbing speed to 105 m/s. The LSMPOWER model determined that this power limit would have to be increased to slightly more than 10 MVA (i.e., by about 40%) for the TR07 to maintain 134 m/s up a 3.5% grade.

Figure 45b shows the maximum speeds that the SCDs and TR07 may maintain up a 10% grade. The values vary considerably: about 5 m/s for

Grumman's baseline design, 90 m/s for Magneplane, 100 m/s for Foster-Miller, and 140 m/s for Bechtel. As with the 3.5% grade results, these are the steady-state balance speeds based on the baseline LSM configurations. For example, the Grumman concept has aluminum conductors for the LSM stator coil. Changing these conductors to copper on the grade portion of the guideway would enable Grumman's optional 100-kN LSM to maintain 125 m/s up a 10% grade.

The TR07 is in a similar situation as the Grumman concept; it cannot maintain much speed (about 14 m/s) up a 10% grade. As with Grumman, however, replacing TR07's aluminum stator windings with copper for the grade section would substantially increase this speed.

LSM stator winding lifetime. The lifetime of the LSM stator winding depends heavily on the thermal stresses to which it is exposed. The motors typically fail when the winding insulation deteriorates, which is accelerated by thermal stresses. A well known practice in electrical machine design is to assume that insulation lifetime halves for each 10°C rise in temperature above its design operating temperature. Industry practice for the design of rotating machinery and bus bars in power installations translates to a current density of about 1.7 MA/m² of conductor cross section.

Figure 46 shows the current density in millions of amperes per square meter for each of the five concepts compared with industry practice. The Grumman, Bechtel, and TR07 current densities are all about 4 MA/m². Magneplane's current density is lowest at about 2 MA/m², and Foster-Miller's is highest at about 6 MA/m².

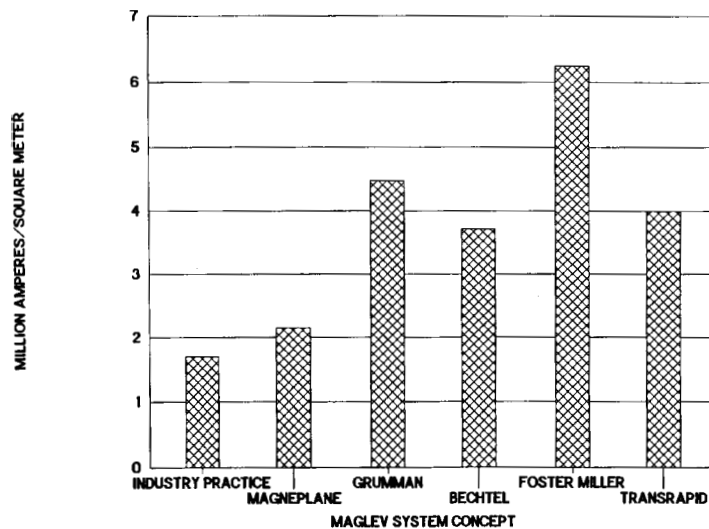


Figure 46. Comparison of the current densities of LSM stator windings.

Not enough is known about the absolute expected lifetime of the LSM stator windings for the duty cycles possible for these systems. However, the above comparisons can be used to estimate the relative stator lifetimes for each of the five concepts. From a thermal stress consideration, the Magneplane LSM should have the longest lifetime, while the Foster-Miller LSM should have the shortest.

LSM stator winding construction. All SCD blocklength LSMs use a stator winding that has overlapping coils, with the coil entrance and exit at the same location on the guideway. This technique is in contrast with the Transrapid Emsland test facility, where the stator coils enter the guideway at the beginning of a block and exit at the end of the block. The advantages of the SCDs' overlapping approach are that it may simplify electrification construction, and it enables a larger pole pitch by having multiple slots (i.e., conductors) per pole. The larger pole pitch in turn lowers the operating frequency of the LSM and the control inverters. This construction technique should improve both performance and cost over the technique used at Emsland.

Efficiency and power factor at electrical source. The converter stations connecting each system to an electrical source differ somewhat. TGV uses AC power directly so that it connects to a source using only a transformer. All other systems connect to a source through solid state AC-DC converters; however, they use the resulting DC power differently.

TR07, Grumman, and Magneplane distribute DC power to widely spaced inverter stations (several kilometers apart). They then use feeder cables to power LSM blocks. Bechtel distributes its high-voltage DC to more closely spaced inverter stations along the guideway. They then power each LSM block using the stator windings as the feeder cables. Foster-Miller distributes lower-voltage DC directly to its LCLSM inverters adjacent to each coil.

We estimated the efficiency and power factor for each system's converter stations and applied these to the output of LSMPOWER to obtain overall values as seen at the electrical source. Table 28 shows a summary of these results for each system. Note that the results for Magneplane include the power-factor correction discussed in their final report.

Table 28. Overall efficiency and power factor for each system at 134 m/s (except TGV-A, which is at 83 m/s).

<i>Parameter</i>	<i>TGV-A (1-10-1)</i>	<i>TR07</i>	<i>Bechtel</i>	<i>Foster-Miller</i>	<i>Grumman</i>	<i>Magneplane</i>
Overall efficiency	0.82	0.83	0.85	0.91	0.78	0.84
Power factor	0.91	0.74	0.98	0.97	0.98	0.99

As expected, Foster-Miller’s LCLSM yields the highest overall efficiency of the concepts studied.

Summary and conclusions

The linear synchronous motor model, LSMPOWER, was developed for two main purposes. First, we used it for an assessment tool to address issues of thrust-speed performance, power and energy consumption requirements, and, to a lesser extent, LSM and related power distribution, power conversion, and control costs. Second, we used it to provide propulsion data to simulate each concept’s operational performance on corridors (section 3.3.1). The model fulfilled both purposes.

An important general finding of this work is that, in virtually all cases, LSMPOWER predicted performance similar to that reported by the SCD studies. More specifically, the GMSA team reached the following conclusions regarding the LSM concepts studied:

- The LSMs considered in all SCD studies, perhaps with the exception of the locally commutated LSM (LCLSM), appear to be technically feasible and are incremental improvements over contemporary designs. However, three of the LSM concepts (Foster-Miller, Grumman, and Magneplane) use the stator as a power transfer component, and the effect of power transfer on LSM performance was not assessed here or in the SCD studies.
- The LCLSM is potentially a major innovation, but it is unproven and requires additional effort to establish its technical feasibility and cost. There are many control issues involved with the LCLSM, and evaluating those issues is beyond the scope of the existing LSMPOWER model. The LCLSM also may require state-of-the art switching devices as part of the power electronics control; the cost of such devices is extremely difficult to predict.

- For both iron-core and air-core LSMs, high efficiencies are attainable. The LCLSM is capable of the highest efficiency because its blocklength is always equal to a consist length.
- The need for feeder cables to energize alternate LSM blocklengths does have some adverse effect on efficiency. It also can significantly reduce the power factor. Both of these increase the cost for electrical energy. Feeder cable requirements can be traded off with more closely spaced converter stations; such trade-off analyses must be part of any route-specific studies.
- The air-core LSMs had the lowest power factors because of the large coil geometries required for the air-core stator coils. Most of the SCD studies recognized the potential need for power factor correction to improve performance. Power factor correction requires more detailed study to assess performance improvement and cost trade-offs. The LSMPOWER model as it currently exists can assess the effects of power correction on performance.
- Acceleration and grade climbing, as expected, require significantly more LSM thrust capability than the steady-state thrust-speed requirements. Meeting these two requirements could significantly and adversely affect both efficiency and power factor. Tailoring the LSM design to meet acceleration and grade climbing performance for route-specific conditions would result in more optimum LSM designs.
- The current density of the LSM is one measure of expected stator-winding lifetime. The SCDs and TR07 all have stator-winding current densities that exceed industry practice (by factors of 1.3 to 4) for what is considered to be conservative, long-lifetime designs. While it is true that, initially, these LSMs will have duty cycle loadings lower than industry practice designs, this advan-

tage may disappear under the close headway operation expected for a mature maglev system. Upgrading the stator windings may be appropriate should this take place.

Recommendations

- The LCLSM requires additional study to establish its technical feasibility. This concept, as envisioned, will make use of computer control to become energized in the propulsion mode at the instant that the superconducting field magnets mounted on the vehicles' bogies are sensed to be present, to synthesize the desired waveforms for driving the LSM coils, and effectively to operate all LSM coils in parallel with equal current sharing. These are control issues that must be addressed. The LCLSM will also function as the power transfer mechanism whenever it is not operating in the propulsion mode; control implications for this power-transfer function should also be examined. These issues are amenable to scale-model evaluation, and such tests should be started immediately to maintain the LCLSM as a viable option. In addition, trade-off studies should determine optimum DC supply voltage and inverter switching speed; both of these have effects on efficiency and cost.
- The power transfer methods that make use of the LSM stator as an inductive coupler are new ideas at the power levels being considered. The feasibility of these concepts to transfer the needed power levels effectively and efficiently, without adversely affecting LSM performance, needs to be established. While many of the questions of feasibility can be addressed analytically, experimental validation of the power transfer techniques is necessary and could be done at the reduced scale.
- The current SCD studies did not quantify the benefits of power regeneration. Regeneration was not assessable at this time in LSMPOWER. We recommend that the analytical and modeling work needed to implement regeneration be done initially through an expansion of the LSMPOWER model and subsequently incorporated into the system simulator.
- Analysis of power-factor correction requires additional effort. All concepts need correction. The specific concepts providing power-factor correction should be investigated

and assessed for both their technical merits as well as their total costs. The current LSMPOWER can model the technical performance effects of various power-factor correction strategies. Existing cost models can be adapted to analyze the total cost.

- The scope and schedule of the recently completed SCD studies limited the choice with linear motors to making incremental improvements over conventional LSM machines. Several experimental linear motors exist that make use of passive field structures. These are attractive because of their potential simplicity over conventional iron-core and air-core LSMs. This could significantly simplify vehicle-carried equipment. Each of these concepts has been shown experimentally to produce thrust, levitation, and guidance forces within a single integrated structure. These machines warrant additional R&D work to determine their performance and costs compared to the more conventional linear motors.

3.2.3 Magnetic fields*

Objectives

Forces resulting from magnetic fields generated both aboard the vehicle and in the guideway are essential for the suspension and propulsion of maglev vehicles. Magnetic fields incidental to these essential functions will exist in the passenger compartment and in regions surrounding the vehicle and guideway. The effects of these fields on passengers and the environment are not well established at this time and so are a matter of concern. Ways of shielding these fields are available, but including them will inevitably increase the weight and cost of the vehicle. In this section, the magnetic forces and stray fields of the TR06/07 maglev system and the four SCDs are analyzed and compared with known and proposed values. These calculations were made to assure that the values presented to the Government are "reasonable." They should not be interpreted as designs or improvements of the concepts analyzed. For expediency, approximate methods have been used in some cases where they serve to verify that the values being checked are credible.

* Written by Dr. Howard Coffey, Center for Transportation Research, Argonne National Laboratory.

Methodology

Methods for calculating electromagnetic fields and forces are well known. However, no single model is adequate for the analysis of all the systems proposed by the SCD contractors. Systems composed of current-carrying coils can be analyzed using straightforward, but sometimes tedious, methods, with the accuracy of the results being limited only by the accuracy with which the input currents and geometries are known. Prudence demanded that simplifications be made in some cases. This method of analysis is appropriate to some electrodynamic maglev systems using simple or "null-flux" coils in the guideway and superconducting magnets on the vehicle. For iron-cored magnets, electrodynamic systems in which the guideway current is induced in continuous sheets, or inter-connected coils such as ladder tracks, however, these methods are insufficient.

A straightforward but complex Dynamic Circuit Theory model computer code, developed by He et al. (1991) of Argonne National Laboratory and verified in part by experiments at ANL (Mulcahy et al. 1993), uses numerical techniques to calculate the time-dependent forces of coil-type suspension systems. This model was used in the analysis of the Foster-Miller concept. A similar model was combined with a harmonic analysis technique to obtain closed-form formulas to analyze the Bechtel concept. Finally, for computing the stray fields from the magnets, He formulated a computer code to calculate the magnetic fields from finite-element conducting filaments in any spatial orientation. The code has been compared to results from the three-dimensional computer code TOSCA with good agreement. These codes are discussed below where they were used.

The analysis of electromagnetic systems containing ferromagnetic materials is complicated by the nonlinear permeability of ferromagnetic materials. For systems in which the magnetic induction is well below the saturation values of the materials used, and for geometries in which the magnetic flux is well confined, the fields and forces can be approximated by analytic formulas. Where this approach is inadequate, which for maglev is generally the case, computer calculations must be made. In making such calculations, a spatial mesh is designed upon which the fields and permeabilities are first approximated and then iterated until a sufficient degree of accuracy is obtained. We used two-dimensional meshes for geometries in which one dimension is extensive

or in which a field geometry is encountered that permits a symmetrical boundary condition to be imposed. More complicated geometries require a three-dimensional mesh and time-consuming computer calculations to obtain reasonable accuracy. Several commercial computer codes are available for this purpose.

Generally, these codes do not provide for cases involving relative motion between the elements of the system. Relative motions result in induced eddy currents in elements of the system that are exposed to time-varying magnetic fields. Since these eddy currents can be substantially reduced by using laminated structures, and since all the ferromagnetic systems analyzed use such structures, this restriction is not believed to be a substantial limitation to the accuracy of the results presented here.

Solutions for the forces in EDS systems that induce the reactive current in a continuous conducting sheet in the guideway have only been obtained for simple geometries in which the sheet forms a closed cylinder or is planar and infinite. Although approximate solutions have been found for some simple geometries, solutions for sheets forming surfaces of finite dimensions must be analyzed using finite-element computer codes similar to those used for ferromagnetic materials but including the motion of the conductor.

Two-dimensional finite-element calculations for simple ferromagnetic structures were made using PE2D, and three-dimensional calculations were made for more complex ferromagnetic structures using TOSCA. All of these are in commercial use and are regarded as reliable. ELEKTRA*, which includes moving media, is relatively new. It is the only commercially available finite-element code of which we are aware that is capable of these computations. It has been used at ANL to calculate the forces on small magnets mounted close to finite, moving, conducting surfaces of various shapes and dimensions (Mulcahy et al. 1993). The results are credible for these small systems. For larger systems, however, a limitation is encountered in the relationship between the velocity and the required distance between nodes in the mesh. For realistic sizes and velocities of maglev magnets, the mesh size becomes extremely small and the number of nodes required becomes prohibitively large for the com-

*The computer codes PE2D, TOSCA, and ELEKTRA are commercial computer codes of Vector Fields, Inc., Aurora, IL.

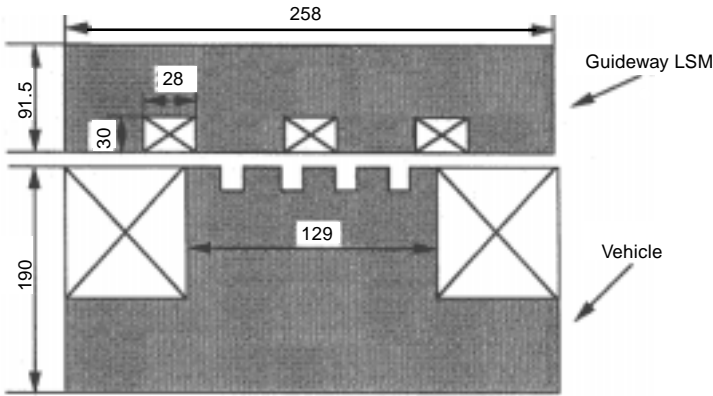
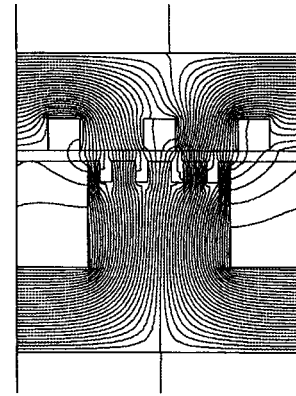


Figure 47. TR06 levitation and propulsion configuration (dimensions in mm).



a. Levitation and propulsion system.

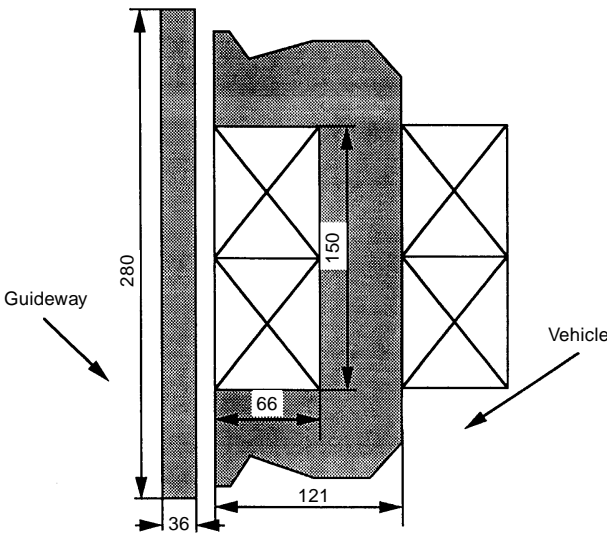
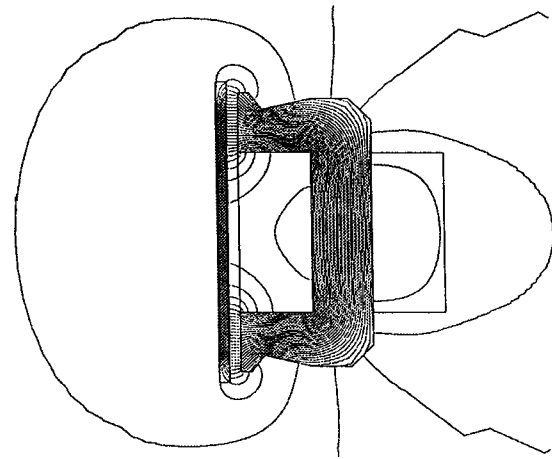


Figure 48. TR07 guidance configuration (dimensions in mm).



b. Guidance system.

Figure 49. TR06 flux patterns.

puters available in this effort. Consequently, only partial results have been obtained for this case.

Application of computational techniques to TR06/07

Data are available for both the TR06 and TR07 systems, which were developed by Transrapid International in Germany (Freidrich et al. 1985, Bohn and Steinmets 1985, Meins et al. 1988, Heinrich and Kretzschmar 1989). These data were used as test cases for the procedures used in the other analyses.

Magnetic forces, TR06. The TR06 two-car vehicle is levitated and propelled using 64 magnets, each 1.3 m long, and having five poles with the approximate dimensions shown in Figure 47. Motion of the vehicle is from the left to the right of the figure. The upper structure is the stator of the linear

synchronous motor and is contained in the guideway. The lower structure or "rotor" is mounted on the vehicle and interacts with the stator to generate both levitation and propulsion forces. The windings in the stator, shown by the large Xs, are the three-phase excitation windings of the LSM. The Xs in the rotor are the excitation windings of the onboard magnets. The slots in the rotor contain additional windings that pick up power from the LSM for onboard use, as discussed in the previous section, and are not considered further. Each magnet comprises five poles, each pole having an excitation current of 6480 AT.

Associated with each levitation magnet is a guidance magnet of equal length and having the approximate dimensions shown in Figure 48. In this figure, the motion is into the page; the flat plate is the vertical reaction rail in the guideway.

The forces in these magnets were modeled using the two-dimensional PE2D computer code. Since the levitation and propulsion forces are interrelated, and depend on the phase currents in the stator winding, the calculations were done with 50% of the maximum phase current in phases A and C and 100% in phase B. The resulting flux patterns are shown in Figure 49, and the data used and the results of the calculations are given in Tables 29 and 30 and Figure 50. They are in reasonable agreement with reported values. The results suggest that the 36,000 AT current reported for TR06 is the maximum rather than the nominal operating excitation current for the system.

Magnetic forces, TR07. The levitation and guidance magnets were changed in TR07, reducing the weight and changing the dimensions. As shown in Figure 51, a notch was placed in the levitation magnets as part of this effort. Our calculated weight exceeds the reported weight by 22%, suggesting that additional, unknown weight reductions were implemented. The levitation magnets were increased in length to 3.022 m and the number of poles per magnet was increased to 10. The pole pitch of 0.258 m was retained to maintain compatibility with the LSM stator. The number of levitation magnets was changed to 30. The configuration of the guidance magnets was revised to incorporate the double windings shown in Figure 52 rather than the single windings of Figure 48. In addition, the length of these magnets was doubled from approximately 1.5 to 3.0 m. This change reduced the stray fields from the guidance magnets which, as discussed later, are the major source of external fields from the vehicle in this system. The excitation currents are not well known for either type of magnet; we assumed 4500 AT per pole for the levitation magnets and 8450 AT for the guidance magnets. The resulting flux patterns are shown in Figure 53, and the forces are shown in Tables 31 and 32. These forces for other currents and gaps are shown in Figures 54 and 55.

To good approximations, the lift force F_L and guidance force F_G of TR07 can be fitted by the following equations:

Table 29. TR06 levitation forces.

Specification	PE2D	TR06
Excitation magnet height	0.190 m	0.190 m
Number of magnets	64	64
Excitation/magnet	32,400 AT	36,000 AT
Air gap	0.010 m	0.010 m
Pole pitch	0.258 m	0.258 m
Stator pack		
width	0.185 m	0.185 m
height	0.0915 m	0.0915 m
Current	1200 A	1200 A
Lift force	1284 kN	1196 kN

Table 30. TR06 guidance forces.

Specification	PE2D	TR06
Excitation current	15 A	15 A
Turns	840	unknown
Air gap	0.010 m	0.010 m
Force/magnet	11 kN	9 kN

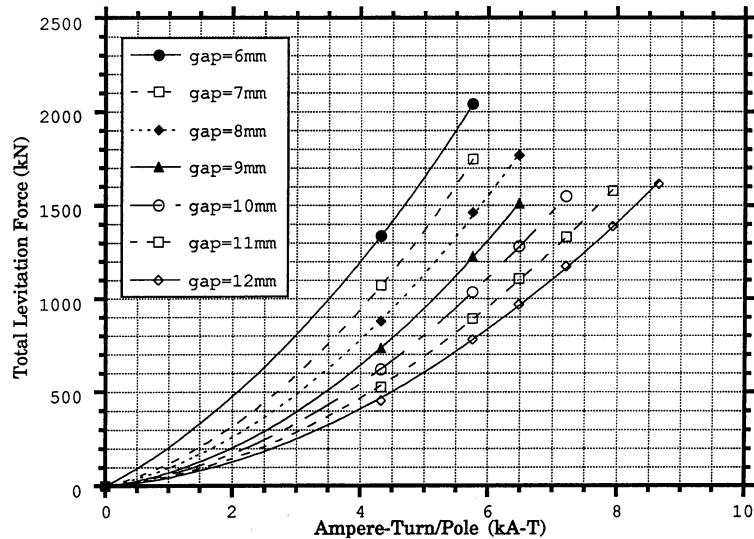


Figure 50. TR06 levitation forces.

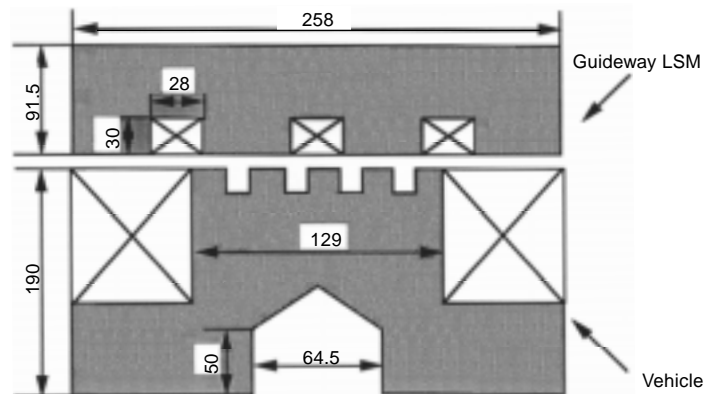


Figure 51. TR07 levitation and propulsion configuration (dimensions in mm).

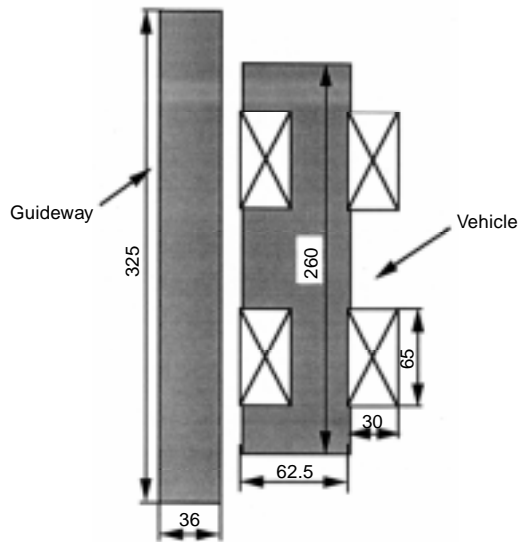


Figure 52. TR07 guidance configuration (dimensions in mm).

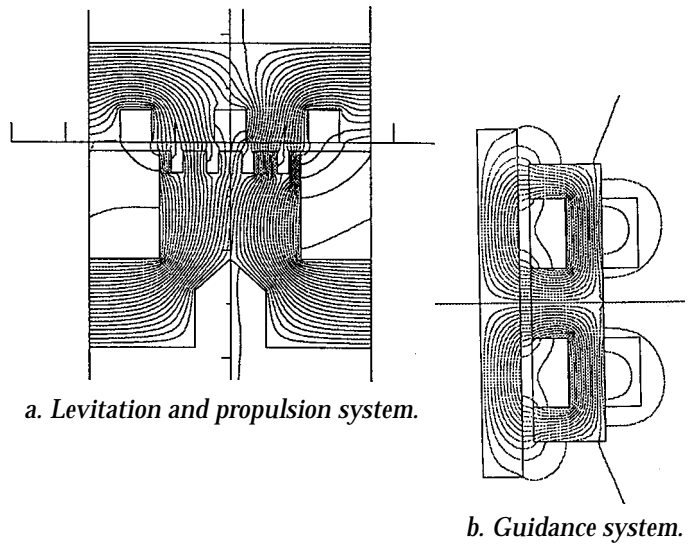


Figure 53. TR07 flux patterns.

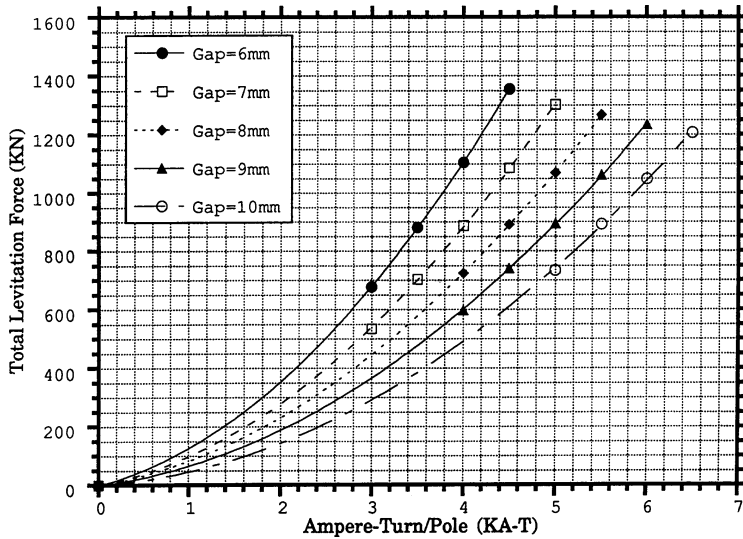


Figure 54. TR07 levitation forces.

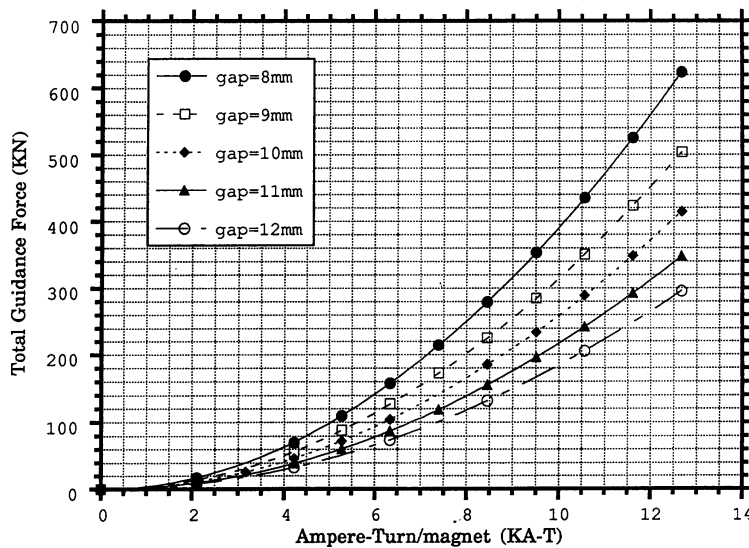


Figure 55. TR07 guidance forces.

Table 31. TR07 levitation force.

Specification	PE2D	TR07
Weight of magnets	14,500 kg	11,800 kg
Number of magnets	30	30
Excitation/magnet	45,000 AT	Unknown
Air gap	0.008 m	0.008 m
Stator current	1200 A	1200 A
Pole pitch	0.258 m	0.258 m
Stator pack		
width	0.180 m	0.180 m
height	0.0915 m	0.0915 m
Lift force	917 kN	882 kN

Table 32. TR07 guidance force.

Specification	PE2D	TR07
Number of magnets	30	30
Weight of magnets	11,600 kg	9,400 kg
Excitation current	8,450 AT	Unknown
Air gap	0.010 m	0.010 m
Force/magnet	12.39 kN	Unknown

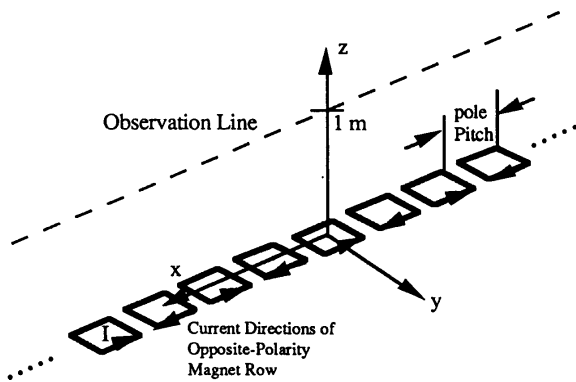


Figure 56. Row of magnets with alternating polarities. (Magnet length = 19.5 cm; magnet width = 24.4 cm; coil current = 45 kAT; pole pitch = 25.8 cm; 20 magnets.)

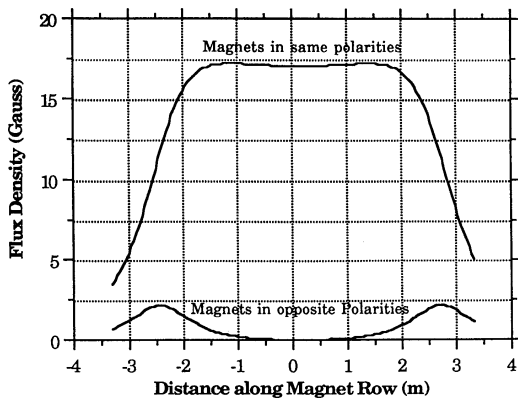


Figure 57. Comparison of magnetic fields from a row of magnets having the same and alternating polarities (magnetic field 1 m above magnet row).

$$F_L = 2337 \cdot (kAT)^{1.876} - 5500 \cdot (kAT)^4 / g^5$$

$$F_G = 180 \cdot (kAT)^2 / g^{1.843}$$

where kAT is the number of kilo-ampere-turns in the windings and g is the gap dimension in meters.

Since no guidance force is generated when the vehicle is in the equilibrium position, the guidance force indicated is that resulting from having the guidance magnets energized on one side and de-energized on the other.

Stray magnetic fields, TR06/07, from levitation-propulsion magnets. The levitation-propulsion magnets of TR06/07 are arranged along the sides of the vehicle and alternate in polarity as required to move the vehicle. The magnetic field at a distance from such an array of magnets is the difference of the fields from the individual magnets. The magnitude of the field depends on the distance from the magnets relative to their lengths, the field being lower if the magnets are short relative to the distance at which the measurement is made. This is illustrated in Figures 56 and 57, where the fields of 20 magnets are calculated at a distance of 1 m above them. From this illustration, the stray fields around the vehicle from this source are expected to be small.

The assumption is better than the figures indicate owing to the presence of iron in the system. Although this analysis would be best if done with a detailed, three-dimensional magnetic model including iron, it does not appear to be necessary in light of this approximate analysis and reported magnetic field measurements made on TR07 (Electric Research and Management, Inc., no date). At the ends of the array, the fields increase. It should be noted that the field from the stator moves with the same velocity as the vehicle and appears to the vehicle as a constant magnetic field. A detailed calculation of the fields in the cabin directly above the levitation magnets is shown in Figure 58.

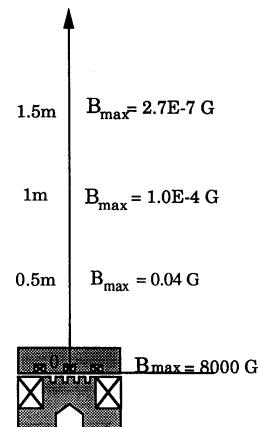


Figure 58. Magnetic fields above TR07 levitation-propulsion magnets.

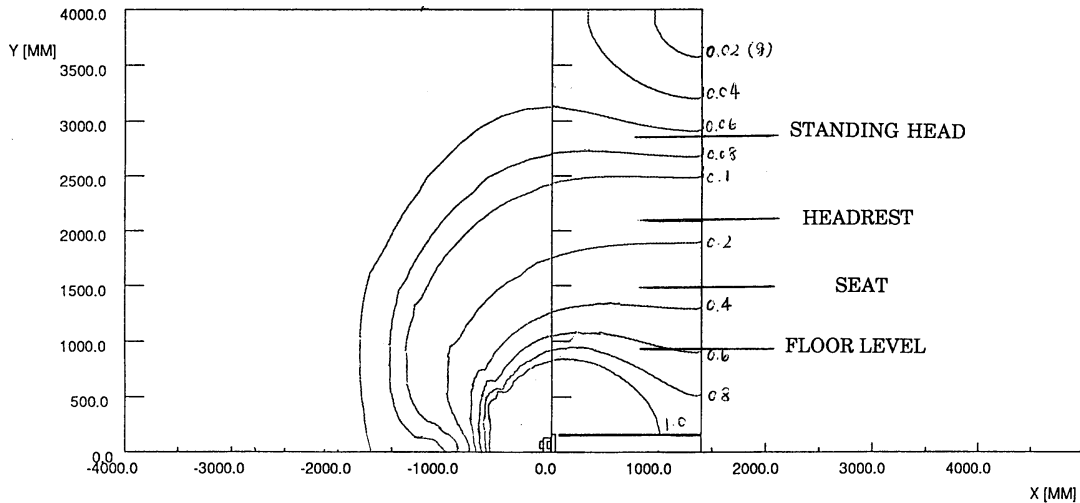


Figure 59. Flux density (G) around TR07 guidance magnet.

Stray magnetic fields, TR06/07, from the guidance magnets. The major source of stray fields in the TR07 system appears to be the guidance magnets. These magnets are 3 m long and therefore do not benefit as greatly, at close distances, from alternation of the poles. As noted above, the configuration of these magnets was changed in TR07, resulting in better confinement and cancellation of fields at large distances. The calculated magnetic fields (in Gauss) at various positions in and around the vehicle are shown in Figure 59. A steel guideway was included in this analysis; an iron-reinforced concrete guideway would alter these stray fields somewhat. The static field of the Earth is about 500 mG and must be added or subtracted from these values to obtain the total static field. The presence, if any, of ferromagnetic materials in the cabin will alter these values. The fields in Table 33 were calculated and are compared with the static fields in the passenger compartment as measured by Electric Research and Management, Inc. (no date).

These fields are shown as static, but will rarely be constant since the vehicle is in motion and the currents in the guidance magnets vary to correct the guidance forces. These variations reflect minor perturbations in the guideway, cornering of

the vehicle, and wind gusts, and perhaps aerodynamic turbulence on the body of the vehicle, and cannot be calculated. The currents in the magnets can be expected to vary by perhaps $\pm 10\text{--}20\%$ in routine operation, leading to AC fields that are this percentage of the static fields. The frequencies of these AC fields will increase as the speed of the vehicle increases, as reflected in the AC measurements made at head level by Electric Research and Management, Inc. (no date) during the operation of TR07. Below about 200 km/hr (55 m/s), the major components of the field were below 100 Hz, while at 400 km/hr (111 m/s) they increased to more than 200 Hz. A prominent, and unexplained, spike of about 15 mG is seen in the 400-km/hr data at about 10 Hz.

In the data presented in Table 34, the values again peak at floor level, suggesting that most of the fields are generated by the magnets and wiring at or below floor level.

Wiring to the control system, as well as other electrical equipment in the vehicle, can contribute fields of the same magnitude in the cabin if they are not adequately shielded. These include wiring for hotel power, electronic converters, etc. A single straight wire carrying 1 A will generate a field of 2 mG at a radius of 1 m, decreasing

Table 33. Magnetic fields (mG) in the TR07.

	Calculated	Measured		
		Minimum	Mean	Maximum
Floor	700	150	820	1500
Seat	300	50	610	1100
Headrest	150	210	620	1020
Standing head	75	150	500	950

Table 34. ERM magnetic field data (mG) for all frequencies from 5–2560 Hz.

	Minimum	Mean	Maximum
Floor	30	100	255
Seat	20	50	140
Headrest	10	30	75
Standing head	≈ 7	20	55

inversely with the radius. Since the guidance magnets operate at a nominal 15 A, the cables to these magnets could contribute 30 mG DC at 1 m and 15 mG DC at 2 m if not shielded, and some fraction of these fields will appear as AC fields in the same manner as the fields generated by the guidance magnets. The same is true of currents to the levitation magnets (of unknown magnitude) and of the AC currents to onboard equipment. These cables have apparently been shielded, or used in pairs for cancellation, since fields of this magnitude do not appear in the data. If they have not been shielded, doing so is a minor matter.

Application to SCD concepts

As noted earlier, there are considerable differences in the designs presented by the four SCD contractors, and no single model suffices to analyze all of them. The methods of calculation used and the results are presented in this section.

The Bechtel concept uses no ferromagnetic materials but does have a ladder guideway that is not amenable to direct analysis by the dynamic circuit theory model, PE2D, or TOSCA. The dynamic circuit theory model was modified to include the LSM waveform as a continuous sine wave extending the length of the vehicle. This is analogous to the approach used in conventional motor theory. It is an approximation in that higher order harmonics, eddy currents in the coils, and the end effects resulting from the finite lengths of the magnets are not included. Nevertheless, the model approximates the results of the contractor and indicates the “reasonableness” of their computations. A separate computer program was written to analyze the null-flux guidance forces in this system.

The Foster-Miller concept uses no ferromagnetic materials or continuous conducting sheets and can be analyzed with reasonable confidence using the dynamic circuit theory model. This model was used to calculate the lift, propulsion, and guidance forces resulting from the interaction of the superconducting magnets aboard the vehicle with null-flux and propulsion coils in the guideway. Stray fields were calculated using the discrete current-carrying element model.

The Grumman concept uses ferromagnetic materials for suspension, guidance, and propulsion and was analyzed as described above for the TR06/07 system. Unlike the Transrapid systems, however, the gap in the ferromagnetic circuit is 40 mm rather than 8–10 mm, resulting in more flux leakage in the gap and requiring three-

dimensional analyses using the TOSCA program.

The Magneplane concept uses continuous sheet guideways that cannot be analyzed with significant accuracy by simple means, requiring that the previously mentioned ELEKTRA computer code be used. Also, as mentioned earlier, the number of mesh elements that could be used was restricted and limited results were obtained. The contractor did not present the methods by which their forces were calculated. Stray fields have been calculated for the vehicle at rest, which represents the worst case.

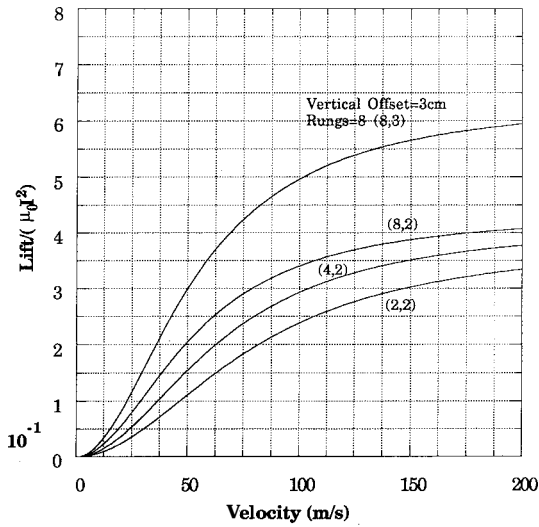
Bechtel

Unique features. The Bechtel concept (see Fig. 3) is unique in that it uses a ladder type of guideway and an array of onboard magnets with alternating polarities to effectively achieve a “null-flux” configuration. When the onboard magnets are symmetrically located with respect to the centerline of the ladder track, no net flux is experienced by the ladder track, and no currents or forces result. The equilibrium operating position of the magnets is a few centimeters below this centerline.

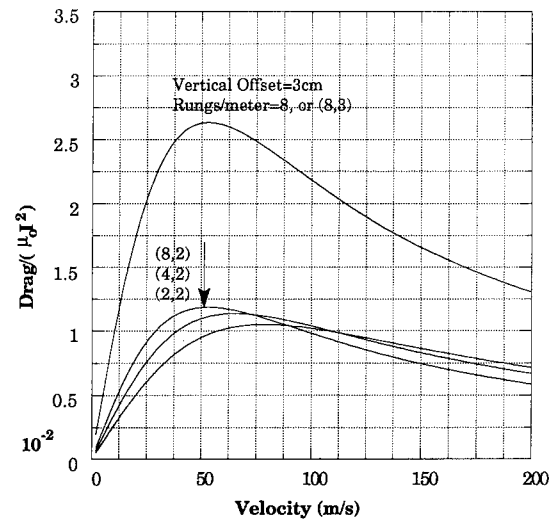
The 96 magnets aboard the vehicle in this system are contained in six modules on each side of the vehicle, the 1-m-long and 0.3-m-wide magnets being positioned with their planes in the vertical direction. The modules are spaced 1 m apart along the length of the vehicle, each module containing eight magnets arranged so that each magnet is adjacent to other magnets with different polarities. The modules are 4 m long and 0.6 m wide.

Adaptations of model for analysis. The dynamic circuit model was used in combination with a harmonic analysis to evaluate the lift and drag forces of the Bechtel design. A steady-state circuit approach was used in the model and provides closed-form analytical solutions that are well suited for the analysis of coil type EDS systems. Guidance in this system is derived from interactions of the onboard magnets with the null-flux guidance coils, with the levitation ladder, and with the propulsion motor. The interaction with the null-flux coils provides the dominant guidance force. The octapole magnets on the vehicle interact with figure-eight-shaped null-flux coils in the guideway that are connected in series with corresponding coils on opposite sides of the guideway.

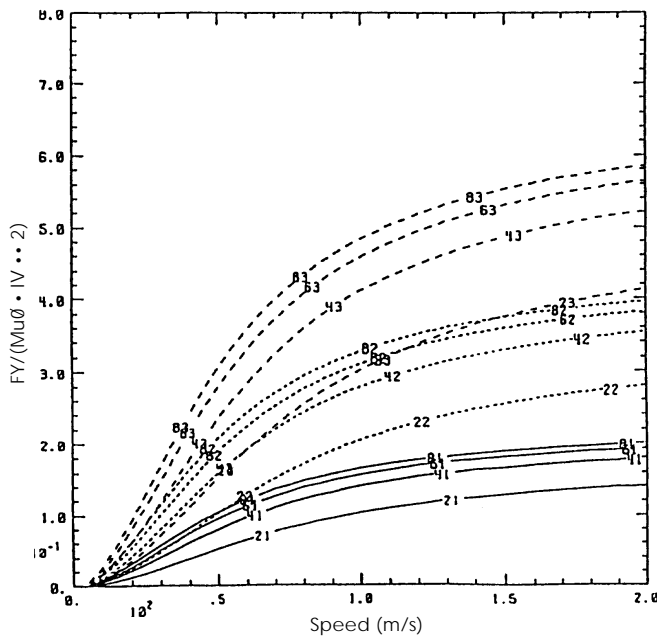
Modeling results for levitation and guidance. The results of the model lift force calculations are shown in Figure 60a, in which the forces are nor-



a. Model lift force calculations.

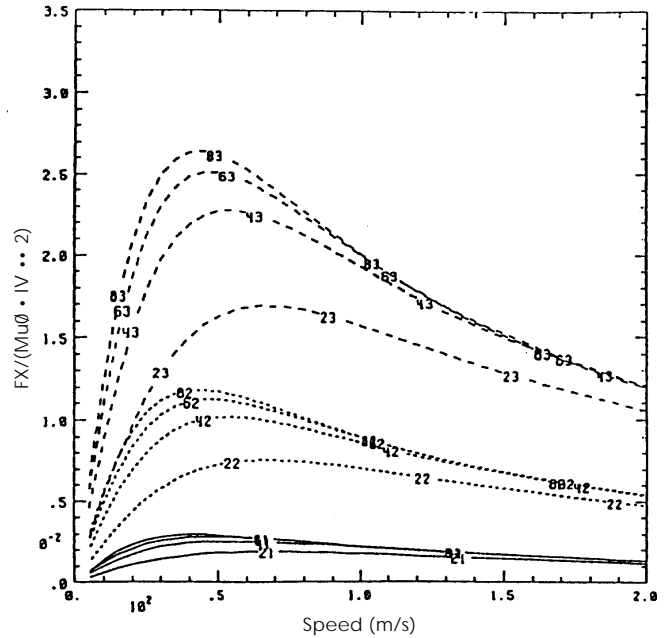


a. Model lift force calculations



b. Bechtel's results.

Figure 60. Normalized lift vs. speed for Bechtel concept, with rung number and vertical offset as parameters. The notation 8,3 etc., refers first to the number of rungs per meter in the ladder guideway and second to the displacement in centimeters of the vehicle-mounted magnets below the centerline of the ladder.



b. Bechtel's results.

Figure 61. Normalized drag vs. speed for Bechtel concept, with rung number and vertical offset as parameters.

malized in the same manner as those presented by Bechtel in Figure 60b as part of their parametric studies. These calculations are for an array of four coils for comparison with the corresponding calculations by Bechtel. The upper and lower horizontal rails of the ladder used in these calculations are 0.030 m high and 0.020 m thick, while the

rungs, or vertical members of the ladder, are 0.01 m wide and 0.020 m thick. Bechtel does not give details of their calculation or the model used. In our calculations, the skin effect is ignored, which is appropriate if the lamination technique proposed by Bechtel is successful. Furthermore, our calculations consider only the first harmonic

of the waveform. Consequently, we adjusted the effective resistivity in our model to obtain the agreement shown. The resistivity remains within a factor of two of its expected value, and the adjustment is in the direction that makes the Bechtel calculation more conservative than ours. Figure 61 shows the resulting drag forces.

The lift and drag forces, lift-to-drag ratio, and the ladder-interaction guidance force resulting from one of the six bogies composed of two mag-

net modules, one on each side of the vehicle (16 magnets per bogie), are shown in Figure 62 as functions of the vertical offset of the magnets from the centerline of the ladder track. The same parameters are plotted in Figure 63 as functions of the vehicle speed.

At 134 m/s, the vertical offset will be about 0.030 m to support the 61,000-kg vehicle. The offset will be greater at lower speeds. The model calculates a lift-to-drag ratio of 140 at 134 m/s.

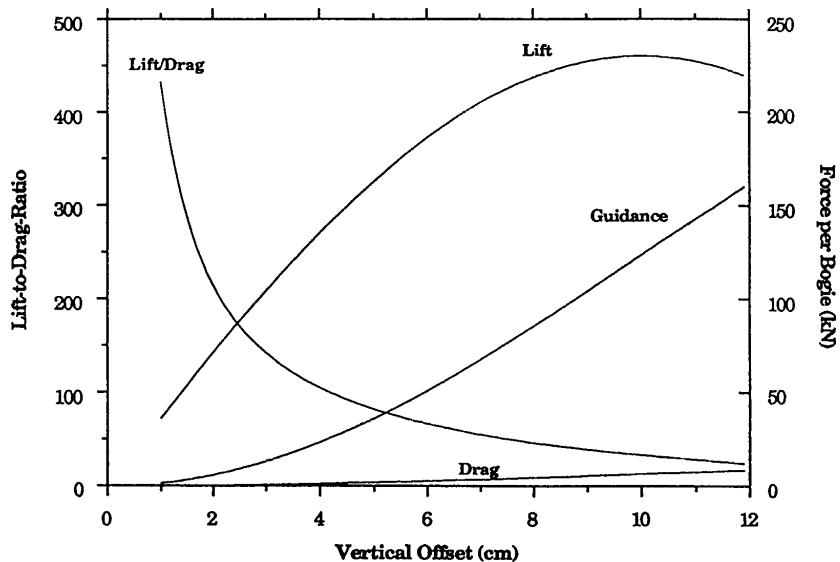


Figure 62. Magnetic force vs. vertical displacement for Bechtel concept (8 rungs/m; 0.20-m gap; 400-kAT magnetic current; 16 magnets/bogie).

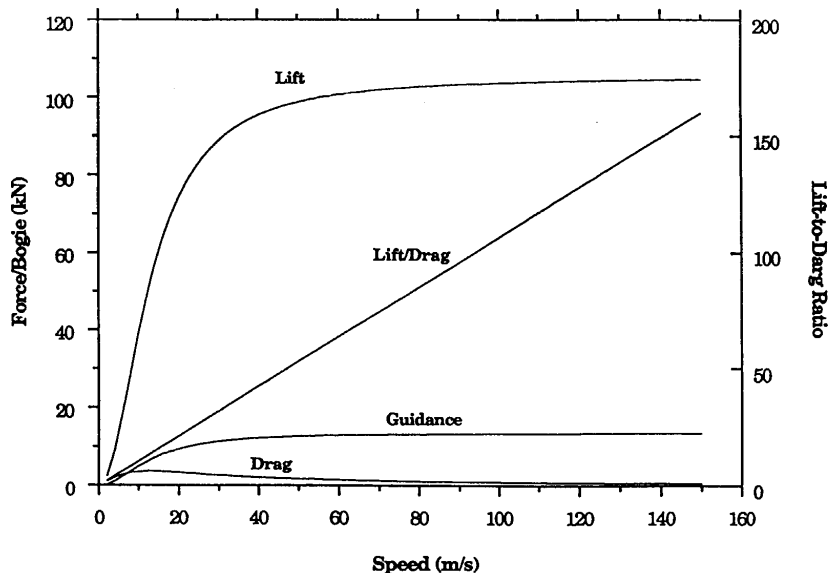


Figure 63. Magnetic forces vs. speed for Bechtel concept (8 rungs/m; 0.20-m gap; 400-kAT magnetic current; 16 magnets/bogie).

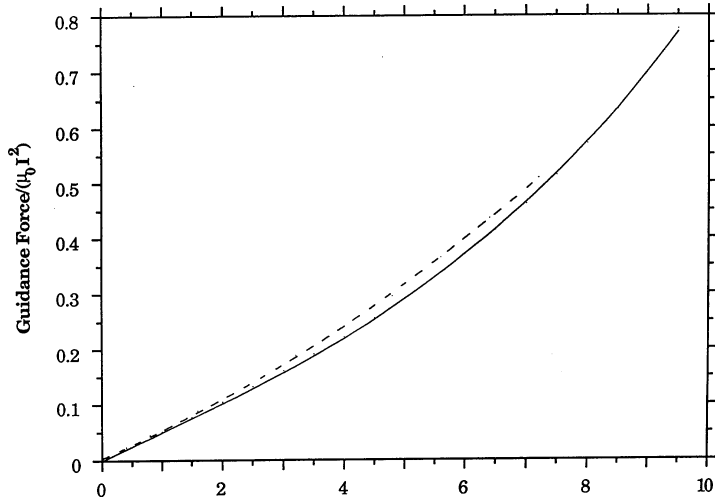


Figure 64. Guidance force vs. lateral displacement for Bechtel concept. Normalized guidance force is acting on eight SCMs, with four on the left and four on the right (solid line shows Argonne results; dashed line shows Bechtel results).

Bechtel calculated power losses in the coils to be 630 kW at this speed, leading to a lift-to-drag ratio of 130 in the absence of eddy current losses or 110 including such losses.

The primary guidance force from the null-flux coil interaction is shown in Figure 64 as a function of the lateral displacement (based on the dimensions given on page B-35 of the Bechtel [1992a] report) and compared with the forces reported by Bechtel (1992a) in their Figure D1-6c. The forces shown for their calculation are the result of summing the separate forces on the two sides of the bogie. The cross-sectional area and conductivity of the conductor were not reported and have been adjusted within physically permissible limits to achieve the agreement shown. A value of 0.1 on the scale shown corresponds to 20 kN for an eight-magnet bogie, resulting in 240 kN of restoring force for the entire vehicle when it slips to the side by 0.02 m.

Modeling results for stray fields. Stray fields for the Bechtel system were computed using the computer code, mentioned earlier, that sums the magnetic fields from each of the finite length current elements of the array of magnets. For simplicity, we considered the magnets to be arranged in a continuous line along each side of the vehicle, whereas each 4-m-long magnet module is actually separated from the next by a distance of 1 m. The effect of considering the magnet modules as continuous rather than spaced apart is to ignore the ballooning of the magnetic field between adjacent modules. This effect will be less than the “end effect” shown in Figure 57 since in that figure the magnet array was not continued beyond the end, while in this case the “end” is followed by another magnet array. The actual “end effect” around the vehicle is shown in Figure 65a, where the fields are calculated along the centerline of the vehicle. The fields in the transverse plane of the vehicle

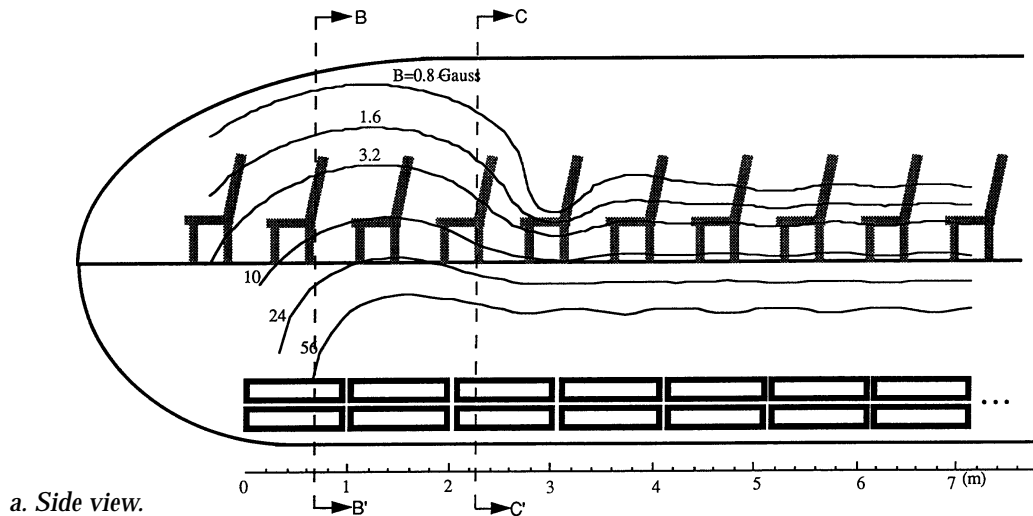
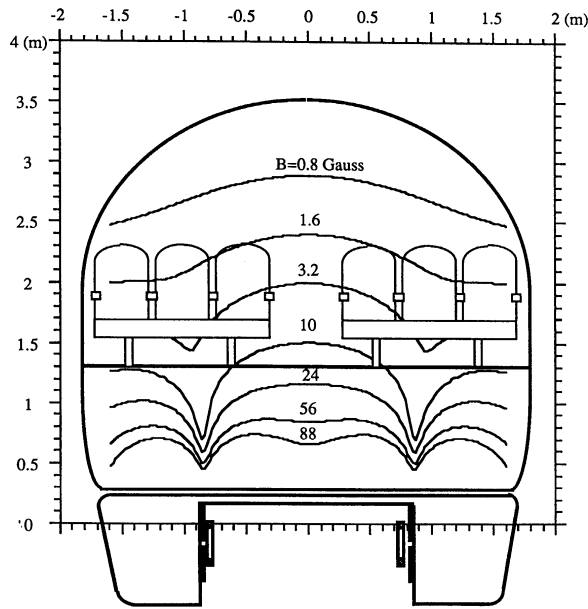
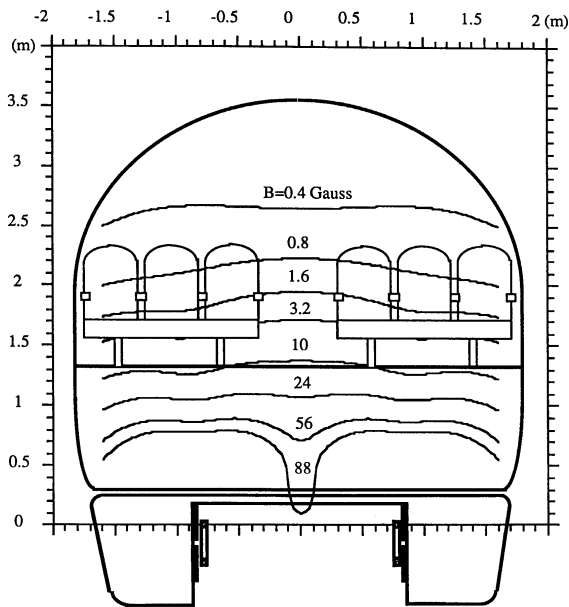


Figure 65. Stray fields along centerline of Bechtel vehicle.



b. Cross-sectional view along B–B' plane. SCM current is 400 kA/coil.



c. Cross-sectional view along C–C' plane. SCM current is 400 kA/coil.

Figure 65 (cont'd).

at cuts B–B' and C–C' are shown in Figures 65b and c. In making these calculations, we assumed the currents to be the same as those used in calculating the magnetic forces. Corresponding calculations from Bechtel are shown in Figure 66. The contours depend on the exact location in the vehicle at which the calculation is made, and

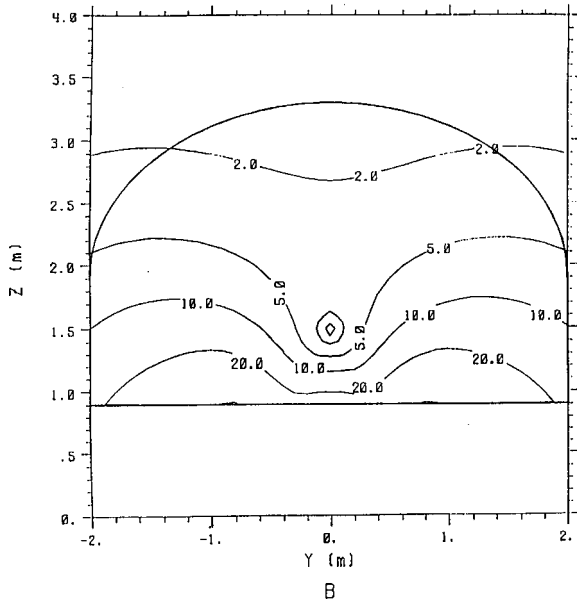
on the polarities of the magnets on opposite sides of the vehicle. The exact arrangement calculated by Bechtel is not known but the magnitudes of the two calculations are in good agreement.

Foster-Miller

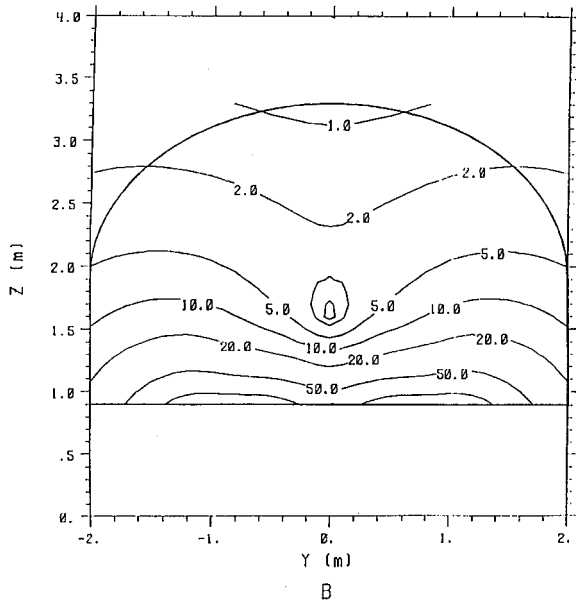
Unique features. The Foster-Miller concept (see Fig. 4) uses racetrack-shaped superconducting magnets on the vehicle that interact with sidewall-mounted coils for levitation, guidance, and propulsion. Levitation, and a portion of the guidance force, is achieved using figure-eight-shaped null-flux levitation coils that are vertically positioned. The vehicle is propelled and guided by a single set of coils that are cross-connected across the guideway and powered in parallel from the way-side. The propulsion system uses a unique locally commutated linear synchronous motor, as discussed in section 3.2.2. The baseline 150-passenger, 73-tonne, 2-car train is levitated and propelled on three bogies. Each bogie contains eight “race-track” shaped superconducting magnets and must generate a vertical force of 238 kN to levitate 24.3 tonnes. Each magnet has a mean winding width of 0.5 m, a mean length of 1.0 m, and 1800 kAT of current. The magnets interact with null-flux coils in the guideway that are 0.74 m long, 0.90 m high, and 0.04×0.04 m in cross section.

Model used for analysis. We used the dynamic circuit theory model, originally developed to analyze null-flux type systems, to directly analyze this system.

Modeling results for levitation and guidance. The magnets aboard the vehicle and the null-flux coils in the guideway must be displaced from their symmetrical positions to generate levitation or guidance forces. The computed levitation forces generated at 134 m/s (300 mph) are shown in Figure 67a as functions of the vertical displacement (offset) and in Figure 67b as functions of the velocity with a 0.035-m offset. This offset achieves the required lift force of 240 kN/bogie at 134 m/s and results in a lift-to-drag ratio of about 180. At 134 m/s, the maximum lift capability of the bogie is about 640 kN, and it occurs at an offset of 0.14 m. The lift-to-drag ratio is significantly lower at this large offset. Foster-Miller's computation of lift vs. deflection (Fig. 68) gives a maximum supportable load of 2.6 times the vehicle weight (essentially the same result as ours). It should be noted that the displacements at takeoff (50 m/s) and landing (20 m/s) will be greater than the 0.035 m discussed here, and the



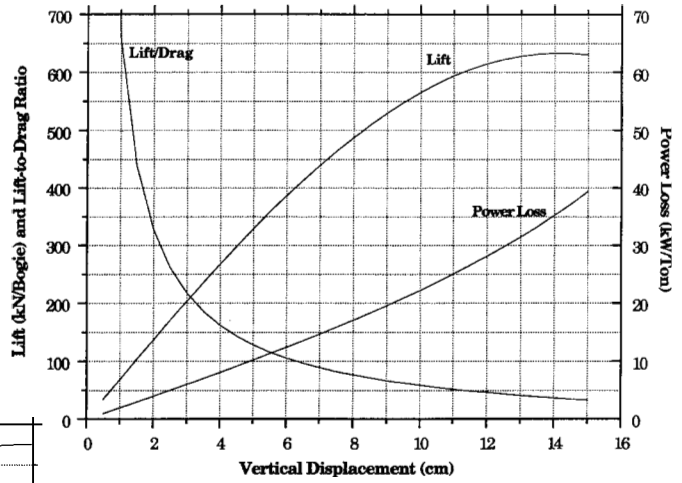
a. Contours of constant magnetic field magnitude (G) along centerline plane.



b. Contours of constant magnetic field magnitude (G) along a plane through the center of the mid-vehicle magnets.

Figure 66. Cross-sectional view of stray fields of Bechtel vehicle (as calculated by the contractor).

a. Versus vertical offset.



b. Versus speed.

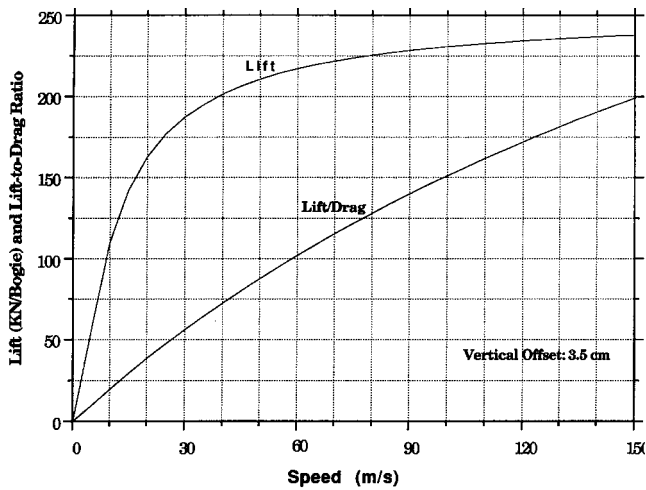


Figure 67. Magnetic suspension force for Foster-Miller concept (27.5-cm gap; 134-m/s speed; 1800-kAT SCM current; 16-cm² conductor cross-sectional area; eight SCMs/bogie).